

Stable cortical body maps before and after arm amputation

Received: 15 July 2024

Accepted: 27 June 2025

 Check for updates

Hunter R. Schone^{1,2,3,4}✉, Roni O. Maimon-Mor^{1,5,6},
Mathew Kollamkulam^{1,7}, Malgorzata A. Szymanska⁸, Craig Gerrand⁹,
Alexander Woollard¹⁰, Norbert V. Kang¹⁰, Chris I. Baker² &
Tamar R. Makin^{1,8,11}✉

The adult brain's capacity for cortical reorganization remains debated. Using longitudinal neuroimaging in three adults, followed before and up to 5 years after arm amputation, we compared cortical activity elicited by movement of the hand (before amputation) versus phantom hand (after amputation) and lips (before and after amputation). We observed stable cortical representations of both hand and lips in primary sensorimotor regions. By directly quantifying activity changes across amputation, we demonstrate that amputation does not trigger large-scale cortical reorganization.

What happens to the brain's map of the body when a part of the body is removed? Over the last five decades, this question has captivated neuroscientists and clinicians, driving research into the brain's capacity to reorganize itself. Primary somatosensory cortex (S1), known for its highly detailed body map, has historically been the definitive region for studying cortical reorganization^{1,2}. For example, foundational research in monkeys reported that, after an amputation or deafferentation, the affected region within the S1 body map suddenly responds to inputs from cortically neighboring body parts (for example, the face)^{3,4}. Additional neuroimaging studies in human amputees supported the theory that amputation of an arm triggers large-scale cortical reorganization of the S1 body map^{5–7}, with a dramatic redistribution of cortical resources, hijacking the deprived territory¹.

Recent studies have challenged this view by harnessing human amputees' reports of experiencing vivid sensations of the missing (phantom) limb. First, human neuroimaging studies demonstrated that voluntary movements of phantom fingers engage neural patterns resembling those of able-bodied individuals^{8–10}. Second, phantom sensations are evoked by cortical¹¹ or peripheral^{12,13} nerve stimulation, suggesting an intact neural representation of the amputated limb, despite its physical absence. Third, neuroimaging studies using both

tactile stimulation and movement paradigms reported no changes in face or lip activity within the deprived cortex of adult amputee participants compared to able-bodied controls^{14,15} (although remapping has been observed in children)¹⁶.

This debate—whether or not amputation triggers large-scale reorganization—remains unresolved^{17,18}, with some suggesting that the two views are not conceptually exclusive, that is, preservation and reorganization can coexist^{5,19,20}. However, a fundamental issue with the evidence on both sides of this debate is a methodological reliance on cross-sectional designs (that is, comparisons between participants). While offering valuable proofs of concept, these studies cannot determine whether the maps of the phantom hand or face are truly preserved or changed relative to their pre-amputation state. To directly track the evolution of cortical representations before and after amputation, we implemented a longitudinal functional magnetic resonance imaging (MRI) approach to track the cortical representations of the hand and face (lips) in three adult participants up to 5 years after arm amputation (Supplementary Video 1), compared with able-bodied control participants (Ctrl) (Fig. 1a). Avoiding the confounding effects of cross-sectional designs²¹, we directly quantified the impact of arm amputation on S1 (re)organization.

¹Institute of Cognitive Neuroscience, University College London, London, UK. ²Laboratory of Brain & Cognition, National Institutes of Mental Health, National Institutes of Health, Bethesda, MD, USA. ³Rehab Neural Engineering Labs, University of Pittsburgh, Pittsburgh, PA, USA. ⁴Department of Physical Medicine and Rehabilitation, University of Pittsburgh, Pittsburgh, PA, USA. ⁵Department of Experimental Psychology, University College London, London, UK. ⁶UCL Institute of Ophthalmology, University College London, London, UK. ⁷Department of Experimental Psychology, University of Oxford, Oxford, UK. ⁸MRC Cognition and Brain Sciences Unit, University of Cambridge, Cambridge, UK. ⁹Department of Orthopaedic Oncology, Royal National Orthopaedic Hospital NHS Trust, Stanmore, UK. ¹⁰Plastic Surgery Department, Royal Free Hospital NHS Trust, London, UK. ¹¹Wellcome Centre for Human Neuroimaging, UCL Institute of Neurology, London, UK. ✉e-mail: schonehunter@gmail.com; tamar.makin@mrc-cbu.cam.ac.uk

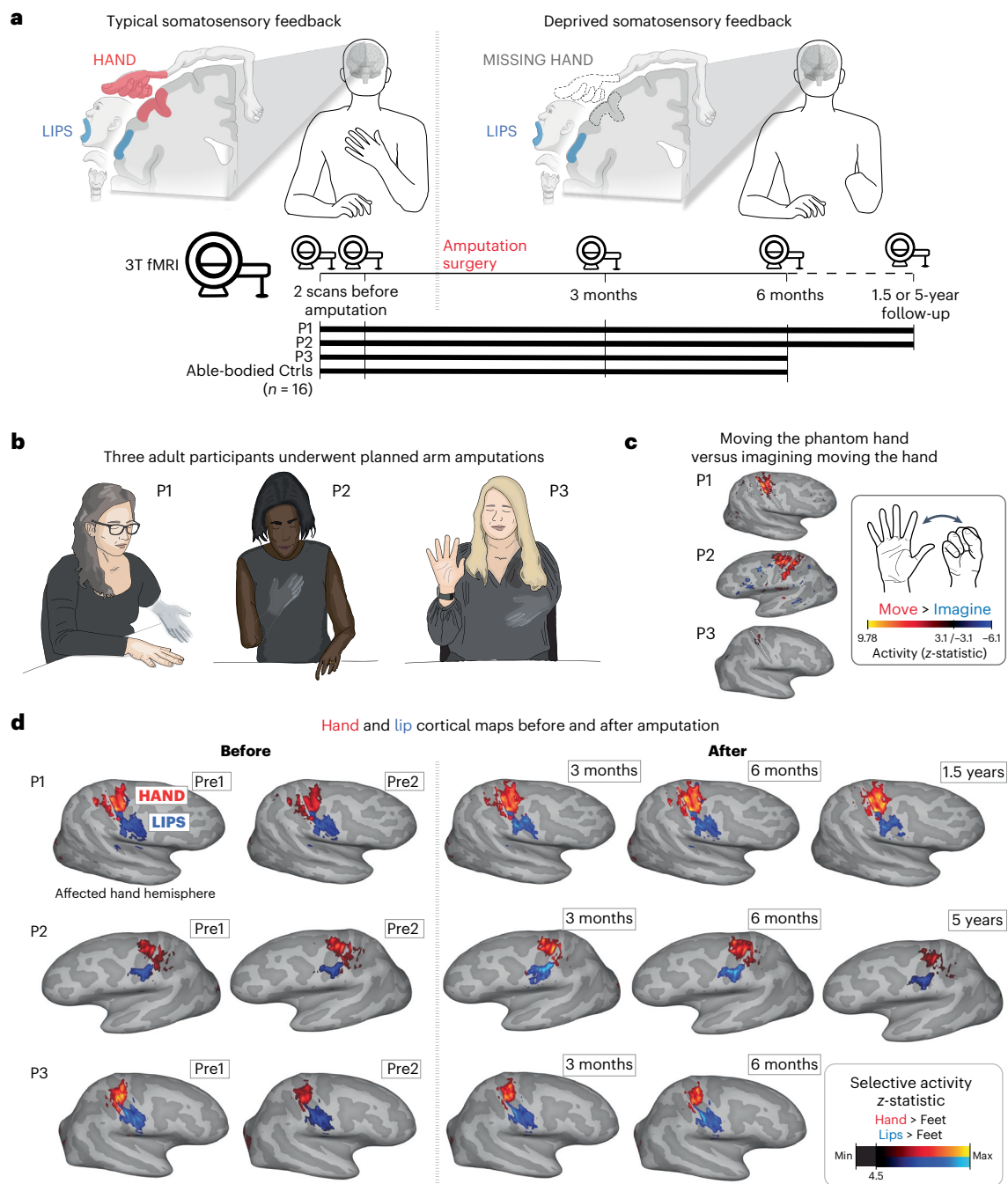


Fig. 1 | Longitudinal investigation of participants with planned arm amputations. **a**, Experimental timeline. Scans before and after amputation were conducted across 4–5 time points: twice before, and at 3 months, 6 months and 1.5 (P1)/5 years (P2) after amputation. **b**, Illustration depicting the three participants 6 months after amputation, including their subjective description of their phantom limb position. **c**, Phantom movements are not imaginary. Univariate activity (z-scored) contrast map displaying a participant's attempts to

open and close the phantom hand versus imagining movement, 6 months after amputation. **d**, Participant's hand (red) and lip (blue) cortical activation maps (contrasted against feet movements) in the affected hand hemisphere across 4–5 sessions. All maps were minimally thresholded at 33% the maximum z-statistic and used a common color scale (the participant's maximum z-statistic > 4.5). Participants agreed to have their image reproduced. Brain illustrations in **a** were created in **BioRender**.

We studied three adult participants (case studies P1, P2 and P3) undergoing arm amputation (demographics in Extended Data Table 1) across 4–5 time points, and 16 able-bodied Ctrls at four time points over 6 months (Fig. 1a). Before amputation, all participants could move all fingers to varying ranges (Extended Data Fig. 1 and Supplementary Video 2). After amputation, all participants reported vivid phantom limb sensations (Fig. 1b), including volitional phantom finger movement (Extended Data Table 1 and Extended Data Fig. 1). Motor control

over the phantom hand was further confirmed by residual limb muscle contractions during phantom movements (Supplementary Video 2), and selective activation in primary sensorimotor cortex for attempted, but not imagined, phantom movements (Fig. 1c). The critical question is to what degree S1 phantom activity reflects the pre-existing hand.

During scanning, participants performed visually cued movements involving tapping individual fingers, pursing lips and flexing toes. Case study participants demonstrated strikingly consistent hand

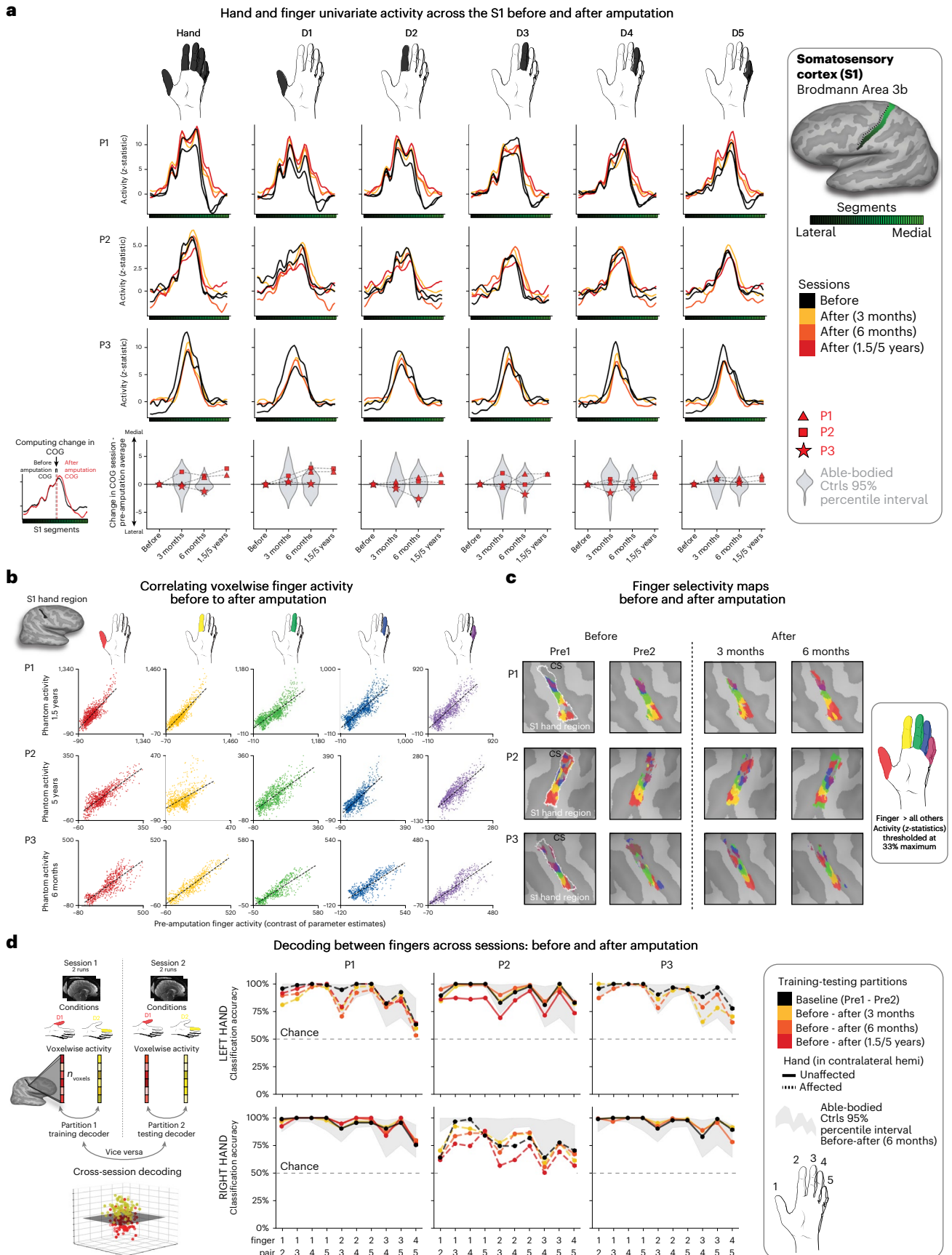


Fig. 2 | Stable hand representation in the affected hemisphere despite amputation. **a**, Longitudinal hand and individual finger activity (versus rest) projected across the S1 (BA3b) region of interest (ROI) segmented into 49 segments of similar height. The affected hand's activity over five sessions (indicated in the legend) for each of the case study participants who underwent an amputation is shown; the bottom row shows the finger COG shifts before and after amputation. The black lines reflect the activity before amputation, the yellow, orange and red lines after amputation. The COG shifts of the case study participants (red) for the hand and individual fingers fell within the distribution of Ctrl (gray; six comparisons per participant; two-tailed Crawford *t*-test: P1 (6 months): $0.14 \leq P_{\text{uncorr}} \leq 0.58$; P2 (6 months): $0.06 \leq P_{\text{uncorr}} \leq 0.81$; P3 (6 months): $0.10 \leq P_{\text{uncorr}} \leq 0.91$). Positive values indicate medial shifts (toward the feet); negative values indicate lateral shifts (toward the lips) in S1. Ctrl 95% percentile interval data are shown as gray violin plots. P1 data are shown as a red triangle. P2 data are shown as a red square. P3 data are shown as a red star. For simplicity, the Ctrl values are all for the left (nondominant) hand. **b**, Before and after amputation single-finger multivoxel correlations: for each finger of the case study participants, voxelwise activity correlations before and at the final scan after amputation are shown. All other correlations are comprehensively

reported in Extended Data Fig. 5. The before to after amputation correlations for all participants were statistically significant (five two-tailed Pearson correlations per participant; P1 (6 months): $0.68 \leq r \leq 0.90$, $P_{\text{uncorr}} < 0.001$; P2 (6 months): $0.80 \leq r \leq 0.85$, $P_{\text{uncorr}} < 0.001$; P3 (6 months): $0.88 \leq r \leq 0.91$, $P_{\text{uncorr}} < 0.001$). **c**, Finger selectivity maps before and after amputation. Each contrast map reflects the selective activity for each finger (versus all others), masked to the hand ROI. Each mask was minimally thresholded at 33% the maximum *z*-statistic and binarized. Color codes are indicated on the right. To visualize the multi-finger activity at a single voxel, a 70% opacity filter was applied to all finger maps. **d**, Left, Graphic illustration of multivoxel analyses using a linear SVM decoder. Right, Longitudinal classifier performance. The line colors denote training-testing cross-validation session pairs, respectively, as indicated in the legend. The gray-shaded area reflects the data of able-bodied Ctrl before and after (6 months) (95% percentile interval). Training the classifier on the pre-amputation data and testing it on the post-amputation data (and vice versa) revealed significantly above chance classification accuracies for all case study participants at all post-amputation sessions (two-tailed, one-sample *t*-test: P1: before 1.5 years: 89%; $P < 0.001$; P2: before 5 years: 67%; $P < 0.001$; P3: before 6 months: 88%; $P < 0.001$). All other annotations are depicted in Fig. 1.

and lip cortical maps before and after amputation (Fig. 1d). Projecting hand and individual finger activity profiles across S1 revealed stable activity before and after amputation, with phantom activity resembling the amplitude and spatial activity spread before amputation (Fig. 2a). A center of gravity (COG) analysis of these profiles revealed spatially consistent hand and individual finger activity in our case studies, with similar pre- and post-amputation session differences over 6 months as Ctrl (six Crawford *t*-tests per participant; P1: $0.14 \leq P_{\text{uncorr}} \leq 0.58$; P2: $0.06 \leq P_{\text{uncorr}} \leq 0.81$; P3: $0.10 \leq P_{\text{uncorr}} \leq 0.91$). Notably, this stability could not be attributed to a pre-existing baseline difference as hand activity before amputation was normal relative to Ctrl (Extended Data Fig. 2a). Similar pre- and post-amputation stability was observed in the motor cortex (M1) (Extended Data Fig. 3a) and for the intact (unaffected) hand (Extended Data Fig. 4a).

Next, we investigated the stability of S1 finger representation in greater detail using a multivoxel pattern analysis (Fig. 2b and Methods). Multivoxel activity patterns for the pre-amputated versus phantom fingers were significantly correlated at 6 months (five Pearson correlations per participant; P1: $0.68 \leq r \leq 0.90$, $P_{\text{uncorr}} < 0.001$; P2: $0.80 \leq r \leq 0.85$, $P_{\text{uncorr}} < 0.001$; P3: $0.88 \leq r \leq 0.91$, $P_{\text{uncorr}} < 0.001$). Correlation coefficients at 6 months fell within the typical distribution seen in Ctrl (see Extended Data Fig. 5 and Supplementary Table 1 for the Ctrl values). Similar stability was observed in M1 (Extended Data Fig. 3b) and for the intact hand (Extended Data Fig. 4c). Combined, this confirmed that activity was largely stable before and after amputation at the single-voxel level.

We next considered finger selectivity, that is, the activity profiles for each finger versus the other fingers. Qualitative finger-mapping revealed preserved somatotopy before and after amputation (Fig. 2c). We applied a multivoxel pattern analysis using a linear

support vector machine (SVM) classifier (Fig. 2d) to explore whether a pre-amputation-trained classifier could decode phantom finger movements (and vice versa). This analysis revealed significantly above chance classification for all case study participants across all post-amputation sessions (Fig. 2d; 2–3 one-sample *t*-tests per participant: P1 (before/1.5 years): 90%; $t_{(9)} = 10.5$, $P_{\text{uncorr}} < 0.001$; P2 (before/5 years): 67%; $t_{(9)} = 4.85$, $P_{\text{uncorr}} < 0.001$; P3 (before/6 months): 89%; $t_{(9)} = 11.0$, $P_{\text{uncorr}} < 0.001$), with similar evidence in M1 (Extended Data Fig. 3c).

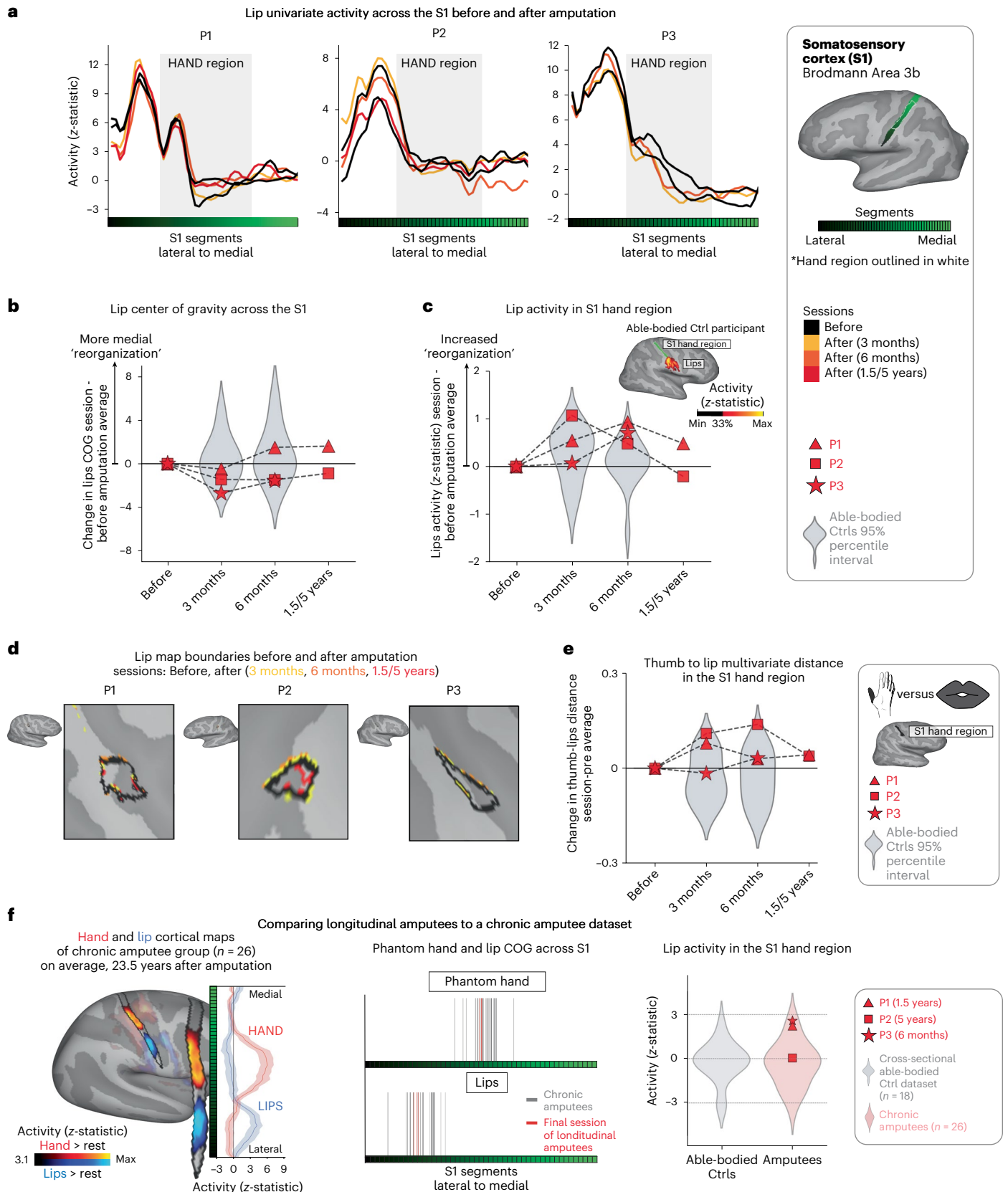
We next investigated whether amputation reduces finger-selective information, as suggested by previous cross-sectional studies²². Assessing for abnormalities in the pre-amputation data, we noted that one of the case study participants, P2, exhibited lower classification for the pre-amputation hand relative to Ctrl (Extended Data Fig. 1), probably because of P2's impaired motor control before amputation (Supplementary Video 2). Our key question remains whether this information degrades further after amputation. When comparing selectivity differences over 6 months relative to Ctrl, none of the case study participants showed significant reductions in average finger selectivity (Crawford *t*-test: P1: $t_{(15)} = -0.34$, $P = 0.73$; P2: $t_{(15)} = -0.24$, $P = 0.80$; P3: $t_{(15)} = -1.0$, $P = 0.33$; Extended Data Fig. 6c). While finger selectivity was reduced at P2's and P3's final scan relative to their baseline (Fig. 2d; three Wilcoxon rank-sum tests per participant: P1 (1.5 years): $W = 3.0$, $P_{\text{uncorr}} = 0.11$; P2 (5 years): $W = 2.0$, $P_{\text{uncorr}} = 0.005$; P3 (6 months): $W = 1.0$, $P_{\text{uncorr}} = 0.01$), these reductions could be attributed to the much greater longitudinal variability between training and testing classifier samples²³. To further explore this, we directly compared the finger selectivity of the affected hand versus the unaffected hand. For two of three of our participants, at the 6-month time point, we observed decreased finger-selective information in the affected hand relative to the unaffected hand, compared

Fig. 3 | No evidence for lip reorganization after amputation. **a**, The lip activity (versus rest) of each case study participant for their sessions projected across the S1 ROI. The black lines reflect pre-amputation activity, with the yellow (3 months), orange (6 months) and red (1.5/5 years) lines reflecting activity after amputation. The gray region depicts the approximated coverage of the hand portion in the S1. **b**, All case study participants showed typical longitudinal variability at their 6-month scan, relative to Ctrl, for the lip COG. Positive values reflect medial shifts (toward the hand). **c**, All case study participants showed typical lip activity in the S1 hand region at the final scan. The right corner depicts representative Ctrl participant activity for the lips (versus the feet) minimally thresholded at 33% the maximum *z*-statistic. **d**, All case study participants exhibited no expansion of the lip map boundaries toward the hand region. Maps were masked to the S1 ROI and were minimally thresholded ($z > 4.5$). **e**, All case study participants showed stable thumb-to-lip multivariate Mahalanobis distances cross-validated

at their final scan, relative to Ctrl. **f**, Comparing the case study participants to a chronic amputee dataset ($n = 26$). Left, Chronic amputee's group-level cortical activation maps of the phantom hand and lips (versus rest) projected onto a single hemisphere (minimally thresholded at $z > 3.1$). Opacity was applied to activity outside the S1 ROI. Group univariate activity was plotted as a line (group mean \pm s.e.) for the phantom hand (red) and lips (blue) across the S1 ROI. Middle, All case study participants, relative to chronic amputees, showed a typical COG for both the phantom hand (top) and lips (bottom). Right, All case study participants exhibited typical lip activity in the S1 hand region during their final session, which is consistent with chronic amputees. The magnitude of lip activity (95% percentile interval) in the S1 hand region for a secondary able-bodied Ctrl group ($n = 18$) is shown in gray. Chronic amputees are shown in light red and the last session data for the case study participants are shown in dark red. All other annotations are the same as described in Fig. 2.

with Ctrl (dominant hand versus non-dominant hand; two Crawford *t*-tests per participant; before 6 months: P1: $P_{\text{uncorr}} = 0.03$; P2: $P_{\text{uncorr}} = 0.03$; P3: $P_{\text{uncorr}} = 0.10$; Supplementary Fig. 1). Collectively across analyses, the decoding results suggested slight (uncorrected) reductions in finger selectivity or increased finger selectivity for the intact hand.

We also performed a complementary representational similarity analysis (RSA) using Mahalanobis distances (a continuous measure of finger selectivity), cross-validated across sessions. Like the decoding, RSA confirmed that finger-selective information was significantly consistent across amputation for all case study participants at all



post-amputation time points (2–3 one-sample t -tests per participant: $P_{\text{uncorr}} < 0.0001$; Extended Data Fig. 6a,b), with similar evidence in M1 (Supplementary Fig. 3c). We noted a few temporary, idiosyncratic (uncorrected) instances of reduced finger selectivity relative to Ctrl (Extended Data Fig. 6c). Using the RSA distances, we also tested the typicality of the inter-finger representational structure, an additional feature of hand representation. Correlating each participant's inter-finger pattern to a canonical pattern revealed no deterioration in typicality scores 6 months after amputation compared to Ctrl, with P3 even showing higher typicality than the Ctrl group (Crawford t -test: P1: $t_{(15)} = -0.9, P = 0.38$; P2: $t_{(15)} = -0.9, P = 0.38$; P3: $t_{(15)} = -3.5, P = 0.003$; Extended Data Fig. 6d). Therefore, despite idiosyncratic reductions in finger selectivity, the representational structure was preserved after amputation.

Finally, we examined changes in lip representation, previously implicated with reorganization after arm amputation^{4,7}. Projecting hand and lip univariate activity onto the S1 segments revealed no evidence of lip activity shifting into the hand region after amputation (Fig. 3a). All case study participants showed typical longitudinal variability at their 6-month scan, relative to Ctrl, for lip COG (Fig. 3b; Crawford t -test: P1: $t_{(15)} = 0.25, P = 0.80$; P2: $t_{(15)} = -0.89, P = 0.38$; P3: $t_{(15)} = -0.9, P = 0.37$). Furthermore, lip activity in the S1 hand region at the final scan was typical (Fig. 3c; P1 (1.5 years): $t_{(15)} = 0.8, P = 0.20$; P2 (5 years): $t_{(15)} = -0.5, P = 0.71$; P3 (6 months): $t_{(15)} = 1.2, P = 0.10$). Also, when visualizing the lip map boundaries within S1 for all sessions, using a common minimum threshold, there was no evidence for an extension of the lip map (Fig. 3d). Examining the multivariate lip representational content, P2 showed an increased lip-to-thumb multivariate distance at their 6-month scan, relative to Ctrl (Fig. 3e; Crawford t -test: P1: $t_{(15)} = 0.69, P = 0.25$; P2: $t_{(15)} = 3.1, P = 0.003$; P3: $t_{(15)} = 0.74, P = 0.23$; intact hand and feet data are included in Extended Data Fig. 7) However, it returned to the typical range of Ctrl when assessed at their 5-year time point. Similar stability was found in M1 (Extended Data Fig. 3) and the unaffected hemisphere (Extended Data Fig. 4). These results demonstrate that amputation does not affect lip topography or representational content in S1.

To complement our longitudinal findings, we compared our case studies to a cohort of 26 chronic upper-limb amputee participants, on average 23.5 years after amputation (Fig. 3f; individual hand and lip cortical maps shown in Extended Data Fig. 8). The topographical features of our case studies were comparable to chronic amputees for both the phantom hand [Crawford t -test: P1 (1.5 years): $t_{(15)} = 0.28, P = 0.77$; P2 (5 years): $t_{(15)} = 0.29, P = 0.77$; P3 (6 months): $t_{(15)} = 0.28, P = 0.22$; $P = 0.82$] and lips [P1 (1.5 years): $t_{(15)} = 0.53, P = 0.59$; P2 (5 years): $t_{(15)} = 0.01, P = 0.98$; P3 (6 months): $t_{(15)} = 0.37, P = 0.71$]. Average lip activity within the S1 hand region was slightly (although not significantly) higher for a few of our case studies relative to chronic amputees [Crawford t -test: P1 (1.5 years): $t_{(15)} = 1.6, P = 0.10$; P2 (5 years): $t_{(15)} = 0.24, P = 0.81$; P3 (6 months): $t_{(15)} = 1.8, P = 0.065$], reflecting that lip activity does not steadily increase in the years after amputation. Collectively, these results provide long-term evidence for the stability of hand and lip representations despite amputation.

Beyond the stability of lip representation across amputation, our findings reveal highly consistent hand activity despite amputation. This unchanged hand representation challenges the foundational assumption that S1 activity is primarily tied to its peripheral inputs, suggesting S1 is not a passive relay of its peripheral input, but an active supporter of a resilient 'model' of the body, even after amputation. Therefore, we conclude that, in the adult brain, S1 representation can be maintained by top-down (for example, efferent) inputs. This interpretation sheds new light on previous studies showing similar S1 topographical patterns activated by touch²⁴, and executed²⁵ and planned movement²⁶.

Because of the limitations of nonhuman models that cannot communicate phantom sensations, it is not surprising that the persistent representation of a body part, despite amputation, has been neglected

in previous studies. Without access to this subjective dimension, researchers may have missed the profound resilience of cortical representations. Instead, previous studies determined S1 topography by applying a 'winner-takes-all' strategy, probing responses to remaining (intact) body parts and noting the most responsive body parts in the input-deprived cortex. Ignoring phantom representations in these analyses leads to severe biases in the interpretation of the area's inputs (as demonstrated in Extended Data Fig. 9). Combined with cross-sectional designs, this has incorrectly led to the impression of large-scale reorganization of the lip representation after amputation. Our longitudinal approach reveals no signs of topographic reorganization in S1, not even subtle upregulation from homeostasis, further reinforcing the notion that S1 is not governed by deprivation-driven plasticity.

For brain–computer interfaces, our findings demonstrate a highly detailed and stable representation of the amputated limb for long-term applications²⁷. For phantom limb pain treatments, our study indicates that targeted muscle reinnervation and regenerative peripheral nerve interfaces do not 'reverse' reorganization or alter the cortical hand representation^{22,28}. Finally, our findings affirm the unaltered nature of adult sensory body maps after amputation, suggesting that Hebbian and homeostatic deprivation-driven plasticity is even more marginal than considered by even the field's strongest opponents of large-scale reorganization^{17,29}.

Online content

Any methods, additional references, Nature Portfolio reporting summaries, source data, extended data, supplementary information, acknowledgements, peer review information; details of author contributions and competing interests; and statements of data and code availability are available at <https://doi.org/10.1038/s41593-025-02037-7>.

References

- Makin, T. R. & Bensmaia, S. J. Stability of sensory topographies in adult cortex. *Trends Cogn. Sci.* **21**, 195–204 (2017).
- Merabet, L. B. & Pascual-Leone, A. Neural reorganization following sensory loss: the opportunity of change. *Nat. Rev. Neurosci.* **11**, 44–52 (2010).
- Merzenich, M. M. et al. Somatosensory cortical map changes following digit amputation in adult monkeys. *J. Comp. Neurol.* **224**, 591–605 (1984).
- Pons, T. P. et al. Massive cortical reorganization after sensory deafferentation in adult macaques. *Science* **252**, 1857–1860 (1991).
- Sparling, T., Iyer, L., Pasquina, P. & Petrus, E. Cortical reorganization after limb loss: bridging the gap between basic science and clinical recovery. *J. Neurosci.* **44**, e1051232024 (2024).
- Makin, T. R. & Flor, H. Brain (re)organisation following amputation: implications for phantom limb pain. *Neuroimage* **218**, 116943 (2020).
- Flor, H. et al. Phantom-limb pain as a perceptual correlate of cortical reorganization following arm amputation. *Nature* **375**, 482–484 (1995).
- Bruurmijn, M. L. C. M., Pereboom, I. P. L., Vansteensel, M. J., Raemaekers, M. A. H. & Ramsey, N. F. Preservation of hand movement representation in the sensorimotor areas of amputees. *Brain* **140**, 3166–3178 (2017).
- Kikkert, S. et al. Revealing the neural fingerprints of a missing hand. *eLife* **5**, e15292 (2016).
- Wesselink, D. B. et al. Obtaining and maintaining cortical hand representation as evidenced from acquired and congenital handlessness. *eLife* **8**, e37227 (2019).
- Mercier, C., Reilly, K. T., Vargas, C. D., Aballea, A. & Sirigu, A. Mapping phantom movement representations in the motor cortex of amputees. *Brain* **129**, 2202–2210 (2006).
- Osborn, L. E. et al. Sensory stimulation enhances phantom limb perception and movement decoding. *J. Neural Eng.* **17**, 056006 (2020).

13. Bensmaia, S. J., Tyler, D. J. & Micera, S. Restoration of sensory information via bionic hands. *Nat. Biomed. Eng.* **7**, 443–455 (2023).
 14. Root, V. et al. Complex pattern of facial remapping in somatosensory cortex following congenital but not acquired hand loss. *eLife* **11**, e76158 (2022).
 15. Valyear, K. F. et al. Interhemispheric transfer of post-amputation cortical plasticity within the human somatosensory cortex. *Neuroimage* **206**, 116291 (2020).
 16. Tucciarelli, R. et al. Shaping the developing homunculus: the roles of deprivation and compensatory behaviour in sensory remapping. Preprint at *bioRxiv* <https://doi.org/10.1101/2024.11.26.624817> (2024).
 17. Makin, T. R. & Krakauer, J. W. Against cortical reorganisation. *eLife* **12**, e84716 (2023).
 18. Ortiz-Catalan, M. The stochastic entanglement and phantom motor execution hypotheses: a theoretical framework for the origin and treatment of phantom limb pain. *Front. Neurol.* **9**, 748 (2018).
 19. Andersen, R. A. & Aflalo, T. Preserved cortical somatotopic and motor representations in tetraplegic humans. *Curr. Opin. Neurobiol.* **74**, 102547 (2022).
 20. Raffin, E., Richard, N., Giroux, P. & Reilly, K. T. Primary motor cortex changes after amputation correlate with phantom limb pain and the ability to move the phantom limb. *Neuroimage* **130**, 134–144 (2016).
 21. Skup, M. Longitudinal fMRI analysis: a review of methods. *Stat. Interface* **3**, 235–252 (2010).
 22. Serino, A. et al. Upper limb cortical maps in amputees with targeted muscle and sensory reinnervation. *Brain* **140**, 2993–3011 (2017).
 23. Ejaz, N., Hamada, M. & Diedrichsen, J. Hand use predicts the structure of representations in sensorimotor cortex. *Nat. Neurosci.* **18**, 1034–1040 (2015).
 24. Sanders, Z.-B. et al. Similar somatotopy for active and passive digit representation in primary somatosensory cortex. *Hum. Brain Mapp.* **44**, 3568–3585 (2023).
 25. Berlot, E., Prichard, G., O'Reilly, J., Ejaz, N. & Diedrichsen, J. Ipsilateral finger representations in the sensorimotor cortex are driven by active movement processes, not passive sensory input. *J. Neurophysiol.* **121**, 418–426 (2019).
 26. Ariani, G., Pruszynski, J. A. & Diedrichsen, J. Motor planning brings human primary somatosensory cortex into action-specific preparatory states. *eLife* **11**, e69517 (2022).
 27. Downey, J. E. et al. A roadmap for implanting electrode arrays to evoke tactile sensations through intracortical stimulation. *Hum. Brain Mapp.* **45**, e70118 (2024).
 28. Socolovsky, M., Malessy, M., Lopez, D., Guedes, F. & Flores, L. Current concepts in plasticity and nerve transfers: relationship between surgical techniques and outcomes. *Neurosurg. Focus* **42**, E13 (2017).
 29. Wandell, B. A. & Smirnakis, S. M. Plasticity and stability of visual field maps in adult primary visual cortex. *Nat. Rev. Neurosci.* **10**, 873–884 (2009).
- Publisher's note** Springer Nature remains neutral with regard to jurisdictional claims in published maps and institutional affiliations.
- Open Access** This article is licensed under a Creative Commons Attribution 4.0 International License, which permits use, sharing, adaptation, distribution and reproduction in any medium or format, as long as you give appropriate credit to the original author(s) and the source, provide a link to the Creative Commons licence, and indicate if changes were made. The images or other third party material in this article are included in the article's Creative Commons licence, unless indicated otherwise in a credit line to the material. If material is not included in the article's Creative Commons licence and your intended use is not permitted by statutory regulation or exceeds the permitted use, you will need to obtain permission directly from the copyright holder. To view a copy of this licence, visit <http://creativecommons.org/licenses/by/4.0/>.
- © The Author(s) 2025

Methods

Our key methodology involved longitudinal comparisons across amputation. This approach was designed to overcome known limitations in cross-sectional designs, where inter-participant variability could spuriously influence group comparisons, particularly when considering small group sample sizes or small effects. An important additional consideration regarding reorganization research in amputees is the difficulty to interpret whether sensorimotor activity for the missing (phantom) hand reflects preserved representation (that is, whether it reflects the same representational attributes as the physical hand before amputation), or an altered hand representation, which exhibits canonical hand representation features, albeit distinct from the pre-amputation hand. The main limitation of longitudinal designs is the contribution of any time-related effects, for example, because of changes in magnetic resonance scanning hardware³⁰ or participants' experience (for example, familiarity with the study environment³¹), which are not directly related to the amputation. To account for nonrelated variables, we also scanned our case studies and Ctrl participants over a similar time frame. For two of our case studies, we had an opportunity to follow up on our procedures after an extended period (1.5/5 years after amputation). As this was not planned in the original design, we were unable to obtain related time points in ourCtrls. Therefore, all comparisons to the Ctrl cohort are focused on the 6-month post-amputation time point.

Participants

Longitudinal case study participants who underwent an amputation. Over a 7-year period and across multiple NHS sites in the UK, we recruited 18 potential participants preparing to undergo hand amputations. Because of many factors (for example, MRI safety contraindications, no hand motor control, age outside the ethics range, high level of disability), we could only perform pre-amputation testing on six volunteers. Because of additional factors (complications during surgery, general health, retractions), we successfully completed our full testing procedure on three participants (for participant demographics, see Extended Data Table 1).

Pre-amputation scans for P1 and P2 were collected 24 h apart and within 2 weeks of their amputations. P3 had a 2.5-year gap between the pre-amputation scans due to coronavirus disease-related delays in testing and in scheduling uncertainty related to their amputation surgery. Their amputation surgery took place 3 months after their second pre-amputation scan.

Case study participant amputation surgeries. There are noteworthy differences in the amputation surgeries of the three case study participants. P1 underwent an amputation to combat a rapidly developing arteriovenous malformation in the upper arm. Before amputation, they had a relatively high level of motor control in the pre-amputation hand. Additionally, P1's amputation included more advanced surgical techniques, involving a combination of targeted muscle reinnervation³² and regenerative peripheral nerve interfaces³³. In these approaches, rather than simply cutting the residual nerve, the remaining nerves were sutured to a new muscle (targeted muscle reinnervation) or implanted with a nerve graft (regenerative peripheral nerve interface) (in P1's case, the technique varied depending on the muscle; Supplementary Fig. 2). P2 underwent a traditional amputation procedure to remove a sarcoma tumor that had been slowly progressing since 1995. Multiple surgeries of the arm, before the amputation, left them with restricted motor control of the fingers, although still able to move them (Supplementary Video 2). Similarly, P3 was diagnosed with Severell–Martorell syndrome, which had led to their left arm having multiple chronic bone fractures. They underwent a traditional amputation procedure, where the major nerves were left to naturally retract. It is important to note that the diversity of conditions, procedures and postoperative states across

our case studies strengthen the universality of our results, which were consistent across case studies.

Longitudinal able-bodied Ctrl group. In addition to the case study participants who underwent an amputation, we tested a Ctrl group that included 16 older able-bodied participants (nine females; mean age \pm s.d. = 53.1 \pm 6.37; all right-handed). The Ctrl group also completed four functional MRI (fMRI) sessions at the same timescale as the participants who underwent an amputation and were age-matched to P2 and P3. Four additionalCtrls were recruited for this group; however, we did not complete their testing because of dropout and incidental findings captured during the MRI sessions.

Ethical approval for all longitudinal study participants was granted by the NHS National Research Ethics Committee (no. 18/LO/0474) and in accordance with the Declaration of Helsinki (v.2013). Written informed consent was obtained from all participants before the study for their participation, and for data storage and dissemination.

Cross-sectional datasets. From three previous studies (one unpublished study and refs. 14,34), we pooled two cross-sectional fMRI datasets: (1) a group of chronic amputees ($n = 26$) and (2) a secondary group of able-bodiedCtrls ($n = 18$). The chronic amputee group included 26 upper-limb amputee participants (four females; mean age \pm s.d. = 51.1 \pm 10.6; 13 missing the left upper-limb; level of amputation: 17 transradial, eight transhumeral and one at the wrist; mean years since amputation \pm s.d. = 23.5 \pm 13.5). The secondary able-bodied Ctrl group included 18 able-bodied participants (seven females; mean age \pm s.d. = 43.1 \pm 14.62; 11 right-handed). For more information on these datasets, see the Supplementary Methods (<https://osf.io/s9hc2/>).

Longitudinal younger adult able-bodied Ctrl dataset. P1 is younger than the longitudinal Ctrl group. As such, we reanalyzed a previously collected dataset including 22 able-bodiedCtrls of a similar age to P1 (mean \pm s.d. = 23.2 \pm 3.8); each were scanned twice, 1 week apart on the same fMRI task and scanner³⁵.

Questionnaires

Because of a restricted time window for performing the tests before amputation, and the participants' high level of physical discomfort and emotional distress, we were highly limited in the number of assessments we could perform. As such, we primarily focused on the functional neuroimaging tasks. However, in addition, we collected data on multiple questionnaires and had participants perform a functional ecological task.

Kinesthetic vividness. Kinesthetic vividness was quantified for each finger before and after the amputation (When moving this finger, how vivid does the movement feel? Please rate between 0 (I feel no finger movement) to 100 (I feel the finger movement as vividly as I can feel my other hand finger moving)).

Finger motor control. Perceived finger movement difficulty was quantified for each finger before and after amputation (When moving this finger, how difficult is it to perform the movement? Please rate between 100 (I found it as easy as moving the homologous finger in the unimpaired hand) to 0 (the most difficult thing imaginable)).

Pain ratings. Before and after amputation, case study participants were asked to rate the frequency of their pre-amputation limb pain or post-amputation phantom limb pain, respectively, as experienced in the last year, as well as the intensity of the worst pain experienced during the last week (or in a typical week involving pain; Extended Data Table 1). Chronic pain was calculated by dividing the worst pain intensity (scale 0–100: ranging from no pain to worst pain imaginable) by pain frequency (1, all the time; 2, daily; 3, weekly; 4, several times

per month; and 5, once or less per month). This approach reflects the chronic aspect of pain because it combines both frequency and intensity^{36,37}. A similar measure was obtained for painless phantom sensation vividness and stump pain. Participants also filled out the painDETECT questionnaire³⁸. Additionally, before and after amputation, participants reported intensity values for different words describing different aspects of pain, quantified using an adapted version of the McGill Pain Questionnaire³⁹. For each word, participants were asked to describe the intensity between 0 (nonexisting) to 100 (excruciating pain) as it related to each word. We used a larger response scale than standard to allow participants to articulate even small differences in their pain experience (Extended Data Fig. 1).

Functional index. Before and after amputation, case study participants were asked to rate their difficulty at performing a variety of functional activities because of their upper-limb problem, quantified using the Upper Extremity Functional Index⁴⁰.

Ecological task

To characterize habitual compensatory behavior, participants completed a task involving wrapping a present (based on ref. 41). Task performance was video-recorded but is not reported in this paper.

Finger movement task

To qualitatively capture how participants moved when cued to perform individual finger movements, at each session, we asked participants to perform a finger movement task where we cued them to move a single finger. Case study participants were cued to perform unilateral movements of the phantom fingers and intact fingers, and then mirrored the movements of the intact and phantom fingers simultaneously. Task performance was video-recorded and is shown in Supplementary Video 2.

Intact finger kinematic task

To test whether the intact fingers were being moved simultaneously during phantom finger movements, we invited two of the three case study participants back for a separate session to assess the kinematics of the intact fingers. The task setup and data are shown in Supplementary Fig. 4.

Scanning procedures

Each MRI session for the longitudinal cohort consisted of a structural scan, four fMRI finger-mapping scans and two body localizer scans, which we report in this article. The additional cross-sectional datasets are detailed in the Supplementary Methods.

fMRI task design

Finger-mapping scans. The fMRI design was the same as a previous study from our laboratory³⁵, although specific adaptations were made to account for the phantom experience of the case study participants who underwent an amputation (described below). Considering that S1 topography is similarly activated by both passive touch and active movement²⁴, participants were instructed to perform visually cued movements of individual fingers, bilateral toe curling, lips pursing or resting (13 conditions in total). This was performed using PsychoPy (v.2021.1.1). The different movement conditions and rest (fixation) cue were presented in 9-s blocks, each repeated four times in each scan. Additionally, each task started with 7 s of rest (fixation) and ended with 9 s of rest.

To simulate a phantom-like tactile experience for the participants before amputation, the affected hand was physically slightly elevated during scanning such that affected finger-tapping-like movements were performed in the air. Alternatively, for the unaffected hand (before and after amputation), the individual finger movements were performed as button presses on an MRI-compatible button box (four buttons per box) secured on the participant's thigh. The movement of

the thumb was performed by tapping it against the wall of the button box. For the Ctrl participants, half of the participants had the right hand elevated, performing the finger movements in the air, and the other half had the left hand elevated.

Instructions were delivered via a visual display projected into the scanner bore. Ten vertical bars, representing the fingers, flashed individually in green at a frequency of 1 Hz, instructing movements of a specific finger at that rate. Foot and lip movements were cued by flashing the words 'Feet' or 'Lips' at the same rate. Each condition was repeated four times in each run in a semi-counterbalanced order. Participants performed four scan runs of this task. One Ctrl participant was only able to complete three runs of the task for one of the sessions.

Imagery control scans. In each of the two body localizer scans, participants were visually cued to move each hand, imagine moving the affected (case study participants) or nondominant hand (Ctrls), in addition to actual lip, toe (on the affected side only) and arm (on the affected side only) movements. The different movement conditions and a rest (fixation) cue were presented in 10-s blocks and repeated four times in each scan.

MRI data acquisition

MRI images were obtained using a 3T Prisma scanner (Siemens) with a 32-channel head coil. Anatomical data were acquired using a T1-weighted magnetization prepared rapid acquisition gradient echo sequence with the following parameters: repetition time (TR) = 2.53 s, echo time (TE) = 3.34 ms, field of view (FOV) = 256 mm, flip angle = 7 degrees and voxel size = 1-mm isotropic resolution. Functional data based on the blood-oxygenation-level-dependent signal were acquired using a multiband gradient echo-planar T2*-weighted pulse sequence⁴² with the following parameters: TR = 1.5 s, TE = 35 ms, flip angle = 70 degrees, multiband acceleration factor = 4, FOV = 212 mm, matrix size of 106 × 106 and voxel size = 2-mm isotropic resolution. Seventy-two slices, with a slice thickness of 2 mm and no slice gap, were oriented parallel to the anterior commissure–posterior commissure, covering the whole cortex, with partial coverage of the cerebellum. Each of the four functional runs comprising the main task consisted of 335 volumes (8 min 22 s). Additionally, there were 204 volumes for the two imagery control scans (5 min 10 s). For all functional scans, the first dummy volume of every run was saved and later used as a reference for coregistration.

fMRI analysis

fMRI data processing was carried out using the FMRIB Expert Analysis Tool (FEAT v.6.0), part of FSL (the FMRIB Software Library, www.fmrib.ox.ac.uk/fsl), in combination with custom bash, Python (v.3) and MATLAB scripts (R2019b, v.9.7, MathWorks, including an RSA toolbox)^{43,44}. Cortical surface reconstructions were produced using FreeSurfer v.7.1.1 (refs. 45,46) and the Connectome Workbench (<https://humanconnectome.org/>) software. Decoding analyses were carried out using scikit-learn v.1.2.2.

fMRI preprocessing

The following prestatistical processing was applied: motion correction using MCFLIRT⁴⁷, non-brain removal using BET⁴⁸, spatial smoothing using a Gaussian kernel of full width at half maximum FWHM of 3 mm for the functional task data, grand-mean intensity normalization of the entire four-dimensional dataset by a single multiplicative factor and high-pass temporal filtering (Gaussian-weighted least-squares straight line fitting, with $\sigma = 90$ s). Time series statistical analysis was carried out using FILM with local autocorrelation correction⁴⁹. The time series model included trial onsets convolved with a double gamma hemodynamic response function; six motion parameters were added as confound regressors. Indicator functions were added to model out single volumes identified to have excessive motion (>0.9 mm).

A separate regressor was used for each high-motion volume (deviating more than 0.9 mm from the mean position). For the finger-mapping scans, the average number of outlier volumes for an individual scan, across all participants, was 1.5 volumes.

To ensure that all longitudinal sessions (Pre1, Pre2, 3 months, 6 months, 1.5/5 years) were well aligned for each participant, we calculated a structural mid-space between the structural images from each session, that is, the average space in which the images were minimally reoriented⁵⁰. The functional data for each individual scan run in a session were then registered to this structural mid-space using FLIRT^{47,51}.

Low-level task-based analysis

We applied a general linear model (GLM) using FEAT to each functional run. For the primary task, the movement of each finger or body part (ten fingers, lips and feet, total of 12 conditions) was modeled against rest (fixation). To capture finger selectivity, the activity for each finger was also modeled as a contrast against the average activity of all other fingers of the same hand.

We performed the same GLM analysis on the six conditions of the imagery scans. To capture the selectivity of actual attempted phantom movements versus imagine phantom hand movements, the activity of the attempted hand movement was also modeled as a contrast against the imagined hand movement.

For each participant, parameter estimates of each of the different conditions (versus rest) and GLM residuals of all voxels were extracted from each run's first-level analysis. All analyses were performed with the functional data aligned to the structural mid-space.

ROIs

S1: Brodmann area 3b. We were specifically interested in testing changes in topography within (and around) Brodmann area 3b (BA3b). First, the structural mid-space T1 image were used to reconstruct the pial and white-gray matter surfaces using FreeSurfer's recon-all. Surface coregistration across hemispheres and participants was conducted using spherical alignment. Participant surfaces were nonlinearly fitted to a template surface, first in terms of the sulcal depth map and then in terms of the local curvature, resulting in an overlap of the fundus of the central sulcus across participants⁵².

S1 (BA3b) hand ROI. The BA3b ROI was defined in the fsaverage template space using probabilistic cytotectonic maps⁵² by selecting all surface nodes with at least 25% probability of being part of the gray matter of BA3b⁵³. Furthermore, for the multivoxel pattern analyses, we restricted the BA3b ROI to just the area roughly representing the hand. This was done by isolating all surface nodes 2.5 cm proximal or distal of the anatomical hand knob⁵⁴. An important consideration is that this ROI may not precisely reflect BA3b for each participant and may contain relevant activity from neighboring S1 areas because of the nature of our data (3T fMRI, smoothing full width at half maximum 3 mm) and the probabilistic nature of the atlas. As such, we considered this as a definitive localizer of S1 and an indicative localizer of BA3b. Surface ROIs were then mapped to the participant's volumetric high-resolution anatomy.

Forty-nine segments of the BA3b. To segment the BA3b into 49 segments, we loaded the fsaverage flattened cortical surface with the boundaries of the BA3b ROI, as defined by the Glasser atlas⁵⁵. We rotated the map so that the central sulcus was perpendicular to the axis. We overlaid a box with 49 segments of equal height on this ROI. By masking the box to the ROI, we constructed the 49 segments of the BA3b ROI. Because this masking approach requires drawing boundary lines using the vertices on the cortical flat map, we could optimally only get 49 segments (maximum) without issues with the boundary drawing approach. These ROIs were then mapped onto the participant's volumetric high-resolution anatomy and further to the participant's cortical surfaces.

M1: Brodmann area 4. The approach for defining the motor cortex ROI was the same as described above, with the sole exception of selecting the Brodmann area 4 region.

Projecting functional activity onto the cortical surface

Using the cortical surfaces generated using recon-all, fMRI maps were projected to the surface using the workbench command's volume-to-surface mapping function, which included a ribbon-constrained mapping method. The cross-sectional datasets were the only exception, where we projected all maps onto a standard cortical surface (Supplementary Methods).

Univariate activity

Contrast maps for moving versus imagine moving the phantom.

To visualize the contrast maps for attempted versus imagine phantom hand movements, estimates from the two imagery control scan runs for the participant's post-amputation (6-month) session were averaged in a voxelwise manner using a fixed-effects model with a cluster-forming z -threshold of 3.1 and family-wise error-corrected cluster significance threshold of $P < 0.05$. Maps were then projected onto each participant's cortical surface. These contrast maps are visualized in Fig. 1c with a minimum z -threshold in both directions of 3.1.

Contrast maps for the hand and lips.

To visualize the contrast maps for the hand and lip movements, estimates from the four finger-mapping scan runs for each session were averaged in a voxelwise manner using a fixed-effects model with a cluster-forming z -threshold of 3.1 and family-wise error-corrected cluster significance threshold of $P < 0.05$. Maps were then projected onto the participant's cortical surface. These contrast maps (hand in red and lips in blue) are visualized in Fig. 1d with a minimum z -threshold of 33% the maximum participant-specific z -statistic.

For completion, the boundaries of the lip maps, for all participants who underwent an amputation across all sessions, are visualized in Fig. 3d. All maps were minimally thresholded at $z > 4.5$ to provide a complementary thresholding approach relative to Fig. 1d.

Hand topography across the 49 segments of the BA3b.

Using the 49 segments of the BA3b (described above), we projected the neural activity for the hand (versus rest) for each hemisphere (contralateral to the hand being moved), session and participant. The average activity across all voxels in each segment was averaged to extract a single value per segment.

COG. To quantify changes in the hand, finger or lip topography, we computed the COG of activity (for a single body part) across the 49 BA3b segments. To do this, we first computed the weighted activity (β_w) across the segments. To do this each segment number was multiplied by the average activity in the segment:

$$\beta_w = (1 \times \beta_1) + (2 \times \beta_2) \dots$$

To compute the COG, we then divided the sum of the weighted activity ($\sum \beta_w$) by the sum of the activity ($\sum \beta$).

$$\text{COG} = \frac{\sum \beta_w}{\sum \beta}$$

When comparing changes in the COG for the hand or a finger, the COG for each post-session was subtracted from the average COG of the pre-sessions (for example, 3-month COG-pre. avg COG). A value greater than zero reflects the COG moving more medially in the post-session compared to the pre-session. A value less than zero reflects the post-session COG being more lateral compared to the pre-session COG.

Finger selectivity maps. To visualize the selectivity maps, estimates from the four finger-mapping scan runs for each session were averaged in a voxelwise manner using a fixed-effects model. When visualizing the clusters, we minimally thresholded each z -statistic at 33% the maximum z -statistic. We stacked the images such that the smallest cluster was the highest overlay (for example, the pinkie finger) and the largest cluster was the underlay. Finally, we applied a 70% opacity to the visualizations to capture multi-finger activity at each voxel.

Representative Ctrl participant body part maps. To provide an example visualization of the activity for each of the body parts shown in Fig. 3c, estimates from the four finger-mapping scan runs for each session were averaged in a voxelwise manner using a fixed-effects model, with a cluster-forming z -threshold of 3.1 and family-wise error-corrected cluster significance threshold of $P < 0.05$. We then visualized the z -statistic map for the contrast of lips > feet and all left fingers > feet on an inflated cortical surface and applied a threshold to each body part ($z > 3.1$).

Lip activity in the BA3b hand region. To test whether there was an increase in lip activity in the BA3b hand region, the average activity for all voxels (non-thresholded) in the ROI was computed for each session and each run. Activity was averaged across runs to compute a session estimate. When testing for a difference between the after and before amputation sessions, the activity for the two pre-amputation sessions was averaged for a pre-amputation average estimate. The activity in each post-amputation session (3 months, 6 months, 1.5/5 years) was then subtracted to the activity of the pre-amputation average.

Winner-takes-all analysis

As a qualitative demonstration of our findings been compatible with previous studies investigating cortical reorganization that used a winner-takes-all approach, we applied a winner-takes-all analysis to S1 functional activity of the case study participants who underwent an amputation. Using each participant's final post-amputation session data, we performed two variations of the analysis including the following conditions: (1) lips, hand and feet; or (2) lips and feet (excluding the hand). Each voxel was assigned exclusively to the condition with the highest activity. The resulting images were mapped to the participant's cortical surface and are visualized in Extended Data Fig. 9.

Multivoxel pattern analyses

We performed several multivoxel pattern analyses that can be broadly categorized into three themes: intra-finger; inter-finger; and inter-body part. In these measures, we were interested in capturing differences within a session and differences between sessions. For all these analyses, we only included voxels in the BA3b hand region.

Intra-finger. Pearson correlations. We first wanted to quantify changes in the pattern of activation for single fingers (intra-finger). We performed Pearson correlations on the beta weights for each finger using data from runs from different sessions (Fig. 2b and Extended Data Fig. 5). For between-session correlations, the beta weights (in our instance, contrast of parameter estimates) for each finger in the four scan runs were separated into partitions, each with two runs, and each set from different sessions. The activity in each two-run set was averaged at every voxel. A Pearson correlation was then performed between the averaged activity in each of the splits. We performed all unique two-run combinations between sessions (36 total combinations) and averaged these correlation coefficients to get a single value per finger. Between-session correlations were performed for all six unique session comparisons: Pre1 to Pre2, Pre1 to 3 months, Pre1 to 6 months, Pre2 to 3 months, Pre2 to 6 months and 3 months to 6 months. Additionally, for P1 and P2, correlations were performed for Pre1 to 1.5/5 years and Pre2 to 1.5/5 years. All correlation coefficients were then averaged and

plotted in Extended Data Fig. 5. For a simpler visualization, we plotted just the first combination for each participant's final scan relative to the pre-amputation average in Fig. 2b.

Inter-finger. We next wanted to quantify changes in the pattern of activation between finger pairs (inter-finger) using a decoding approach (Fig. 2d) and cross-validated Mahalanobis distances (Extended Data Fig. 6). Both approaches capture slightly different aspects of the representational structure⁵⁶, which we elaborate on below.

For these two analyses, the beta weights from the first-level GLM for each participant were extracted and spatially pre-whitened using a multivariate noise normalization procedure (as described in ref. 56). This was done for each scan using the residuals from the GLM. We then used these noise-normalized beta weights for the next analyses.

Decoding. First, we performed a decoding analysis. A strength of this approach is that it provides an estimate for chance performance (50%), that is, it is a classification accuracy significantly greater than chance. For the case study participants who underwent an amputation, the decoding approach can tell us whether a decoder trained on pre-amputated finger pairs can correctly decode the same information on a phantom hand.

We used a linear SVM classifier (scikit-learn v.1.2.2; sklearn.svm, LinearSVC) to quantify the between-session decoding for each finger pair. Default parameters were used for the classifier. Classification accuracy above chance (50%) denotes that there is some amount of shared information between the training and testing datasets.

We trained the classifier on the noise-normalized beta weights for each finger pair (ten in total). The training and testing splits were performed using data from different sessions, such that the classifier was trained on each unique two-run combination from one session and tested on all unique two-run combinations in a separate session (36 combinations for each finger pair). We performed the same classification approach in the reverse direction (72 combinations in total) because the forward and reverse directions provide unique values. The accuracies for each finger pair for each two-run combination for each training and testing direction were then averaged. Between-session accuracies are shown in Fig. 1d.

Cross-validated Mahalanobis distances. Because our decoding analysis was performed at ceiling (close to 100%), we also performed a RSA using cross-validated Mahalanobis distances. The strength of this approach is that it computes a distance measure (continuous) rather than a binary decoding measure. As such, it is arguably more sensitive for capturing the inter-finger representational structure. Larger distances reflect more dissimilar (distinct) activity patterns and smaller distances reflect more similar patterns.

We performed this analysis using data from different sessions to compute between-session distances (our desired measure for representational stability over time). A distance cross-validated between sessions captures the stability of the information content.

We calculated the squared cross-validated Mahalanobis distance between activity patterns as:

$$d^2(x_y, x_z) = (x_y - x_z)_A^T \Sigma^{-1} (x_y - x_z)_B$$

where $(x_y - x_z)_A$ corresponds to the difference between the activity patterns of conditions y (for example, thumb) and z (for example, index finger) in partition A, and Σ refers to the voxelwise noise covariance matrix. We performed this procedure over all possible two-run cross-validation folds and then averaged the resulting distances across folds. There were 36 unique cross-validation folds between sessions. Note that the cross-validated distance gives you the same distance value regardless of whether it is assigned partition A or partition B. Between-session distances are shown in Extended Data Fig. 6.

Typicality. To quantify a measure that represents the degree of ‘normality’ of the hand representation, we computed a representational typicality measure¹⁰. For each participant’s nondominant left hand, we extracted the ten crossnobis distances for the Pre-3 month and Pre-6 month comparisons. We then averaged these vectors across all able-bodied participants to get an average typical hand pattern. We then performed a Spearman rho correlation between the cross-validated Mahalanobis finger-pair distances for each participant’s affected or nondominant (left) hand and the average typical hand pattern. When comparing a Ctrl participant to the Ctrl mean, the respective participant was left out from the estimation of the Ctrl mean distances. These values are depicted in Extended Data Fig. 6.

Inter-body part. Finally, we wanted to quantify changes in the pattern of activation between the thumb, lips and feet in the S1 hand region. We computed the cross-validated Mahalanobis distances between these body parts in the same manner as the inter-finger analysis. The thumb to lips distances are plotted Fig. 3. The distances between all conditions are plotted in Extended Data Fig. 7.

Statistical analyses

All statistical analyses were performed either with Python scripts using `scipy.stats` and `statsmodels.stats.multitest` or JASP (v.0.17.2.1). Normality was ascertained using a Shapiro–Wilk test. For most of the analyses, to test whether a case study participant was significantly different from the Ctrl group, we used Crawford & Howell’s method, which provides a point estimate of the abnormality of the distance of each case from a Ctrl sample⁵⁷. For all Crawford tests, we report uncorrected, two-tailed *P* values. When comparing estimates to zero or chance decoding (50%), we used a two-tailed, one-sample *t*-test. When testing for a decrease in measures within-participant, we used a Wilcoxon signed-rank test. When further testing for differences between hands within-participant, we performed a Wilcoxon signed-rank test on the classification accuracy values and a paired samples *t*-test on the Mahalanobis distances. The resulting *P* values were *z*-transformed and are plotted in Supplementary Fig. 1. Additionally for the correlation analyses, Pearson correlations were used for the intra-finger multivoxel pattern analysis and Spearman correlations were used for the typicality analysis.

Across all our previous studies, we operationally defined amputees’ intact hand as their de facto dominant hand, and as such have always compared the nondominant hand of Ctrl to the missing hand of amputees (for example, see refs. 9,14,37,41,58–60). Therefore, across all case study to Ctrl comparison analyses, we statistically compared (and plotted) the left (nondominant) hand side of Ctrl to the case study participants missing hand side.

Reporting summary

Further information on research design is available in the Nature Portfolio Reporting Summary linked to this article.

Data availability

Data for the primary results have been made publicly available (<https://osf.io/s9hc2/>).

Code availability

The code for the primary results has been made publicly available (<https://github.com/hunterschone/longitudinal-amputation>).

References

30. Lee, H. et al. Estimating and accounting for the effect of MRI scanner changes on longitudinal whole-brain volume change measurements. *Neuroimage* **184**, 555–565 (2019).
31. McGonigle, D. J. et al. Variability in fMRI: an examination of intersession differences. *Neuroimage* **11**, 708–734 (2000).
32. Kuiken, T. A. et al. Targeted reinnervation for enhanced prosthetic arm function in a woman with a proximal amputation: a case study. *Lancet* **369**, 371–380 (2007).
33. Hooper, R. C. et al. Regenerative peripheral nerve interfaces for the management of symptomatic hand and digital neuromas. *Plast. Reconstr. Surg. Open* **8**, e2792 (2020).
34. Tucciarelli, R. et al. Does ipsilateral remapping following hand loss impact motor control of the intact hand? *J. Neurosci.* **44**, e0948232023 (2024).
35. Kieliba, P., Clode, D., Maimon-Mor, R. O. & Makin, T. R. Robotic hand augmentation drives changes in neural body representation. *Sci. Robot.* **6**, eabd7935 (2021).
36. Kikkert, S. et al. Motor correlates of phantom limb pain. *Cortex* **95**, 29–36 (2017).
37. Makin, T. R. et al. Phantom pain is associated with preserved structure and function in the former hand area. *Nat. Commun.* **4**, 1570 (2013).
38. Freynhagen, R., Baron, R., Gockel, U. & Tölle, T. R. painDETECT: a new screening questionnaire to identify neuropathic components in patients with back pain. *Curr. Med. Res. Opin.* **22**, 1911–1920 (2006).
39. Melzack, R. The short-form McGill Pain Questionnaire. *Pain* **30**, 191–197 (1987).
40. Stratford, P., Binkley, J. & Stratford, D. Development and initial validation of the Upper Extremity Functional Index. *Physiother. Can.* **53**, 259–267 (2001).
41. Hahamy, A. et al. Representation of multiple body parts in the missing-hand territory of congenital one-handers. *Curr. Biol.* **27**, 1350–1355 (2017).
42. Uğurbil, K. et al. Pushing spatial and temporal resolution for functional and diffusion MRI in the Human Connectome Project. *Neuroimage* **80**, 80–104 (2013).
43. Nili, H. et al. A toolbox for representational similarity analysis. *PLoS Comput. Biol.* **10**, e1003553 (2014).
44. Wesselink, D. B. & Maimon-Mor, R. O. RSA toolbox extension for FSL (2018).
45. Dale, A. M., Fischl, B. & Sereno, M. I. Cortical surface-based analysis. I. Segmentation and surface reconstruction. *Neuroimage* **9**, 179–194 (1999).
46. Fischl, B., Liu, A. & Dale, A. M. Automated manifold surgery: constructing geometrically accurate and topologically correct models of the human cerebral cortex. *IEEE Trans. Med. Imaging* **20**, 70–80 (2001).
47. Jenkinson, M., Bannister, P., Brady, M. & Smith, S. Improved optimization for the robust and accurate linear registration and motion correction of brain images. *Neuroimage* **17**, 825–841 (2002).
48. Smith, S. M. Fast robust automated brain extraction. *Hum. Brain Mapp.* **17**, 143–155 (2002).
49. Woolrich, M. W., Ripley, B. D., Brady, M. & Smith, S. M. Temporal autocorrelation in univariate linear modeling of fMRI data. *Neuroimage* **14**, 1370–1386 (2001).
50. Reuter, M., Schmansky, N. J., Rosas, H. D. & Fischl, B. Within-subject template estimation for unbiased longitudinal image analysis. *Neuroimage* **61**, 1402–1418 (2012).
51. Jenkinson, M. & Smith, S. A global optimisation method for robust affine registration of brain images. *Med. Image Anal.* **5**, 143–156 (2001).
52. Fischl, B. et al. Cortical folding patterns and predicting cytoarchitecture. *Cereb. Cortex* **18**, 1973–1980 (2008).
53. Wiestler, T. & Diedrichsen, J. Skill learning strengthens cortical representations of motor sequences. *eLife* **2**, e00801 (2013).
54. Yousry, T. A. et al. Localization of the motor hand area to a knob on the precentral gyrus. A new landmark. *Brain* **120**, 141–157 (1997).

55. Glasser, M. F. et al. A multi-modal parcellation of human cerebral cortex. *Nature* **536**, 171–178 (2016).
56. Walther, A. et al. Reliability of dissimilarity measures for multi-voxel pattern analysis. *Neuroimage* **137**, 188–200 (2016).
57. Crawford, J. R. & Howell, D. C. Comparing an individual's test score against norms derived from small samples. *Clin. Neuropsychologist* **12**, 482–486 (1998).
58. Amoroso, E. et al. Reassessing referral of touch following peripheral deafferentation: the role of contextual bias. *Cortex* **167**, 167–177 (2023).
59. Maimon-Mor, R. O. & Makin, T. R. Is an artificial limb embodied as a hand? Brain decoding in prosthetic limb users. *PLoS Biol.* **18**, e3000729 (2020).
60. Maimon-Mor, R. O., Schone, H. R., Moran, R., Brugger, P. & Makin, T. R. Motor control drives visual bodily judgements. *Cognition* **196**, 104120 (2020).
61. Wesselink, D. B. et al. Malleability of the cortical hand map following a finger nerve block. *Sci. Adv.* **8**, eabk2393 (2022).
62. Muret, D. & Makin, T. R. The homeostatic homunculus: rethinking deprivation-triggered reorganisation. *Curr. Opin. Neurobiol.* **67**, 115–122 (2021).

Acknowledgements

We thank our participants for their immense generosity and dedication to contributing to this research. We thank the multiple clinicians who assisted in recruitment, namely: I. Sedki, S. Kirker and D. Henderson Slater. We thank L. Teichmann, H. Dimitrov, M. Vaziri Pashkam and R. Tucciarelli for feedback and support with the analyses. We thank C. Gallay for help with data collection. The study was supported by a Wellcome Trust Senior Research Fellowship (no. 215575/Z/19/Z) awarded to T.R.M., who is also supported by the Medical Research Council (no. MC_UU_00030/10). H.R.S. and C.I.B. were supported by the Intramural Research Program of the National Institute of Mental Health (no. ZIAMH 002893). H.R.S. was also supported by a research fellowship from the National Institute of Mental Health of the National Institutes of Health (no. F32MH139145). This research was supported in part by the Intramural Research Program of the National

Institutes of Health (NIH). The contributions of the NIH author(s) were made as part of their official duties as NIH federal employees, are in compliance with agency policy requirements and are considered Works of the United States Government. However, the findings and conclusions presented in this paper are those of the author(s) and do not necessarily reflect the views of the NIH or the US Department of Health and Human Services.

Author contributions

H.R.S. designed the research, collected the data, analyzed all the datasets and wrote the manuscript. T.R.M. and C.I.B. designed the research, supervised the analyses and edited the manuscript. M.K. helped collect the data, preprocessed the cross-sectional datasets and edited the manuscript. M.A.S. helped with collecting the data and edited the manuscript. R.O.M.M. designed the research, collected the data, supervised the analyses and edited the manuscript. C.G., A.W. and N.V.K. were involved in recruitment and editing the manuscript.

Competing interests

The authors declare no competing interests.

Additional information

Extended data is available for this paper at <https://doi.org/10.1038/s41593-025-02037-7>.

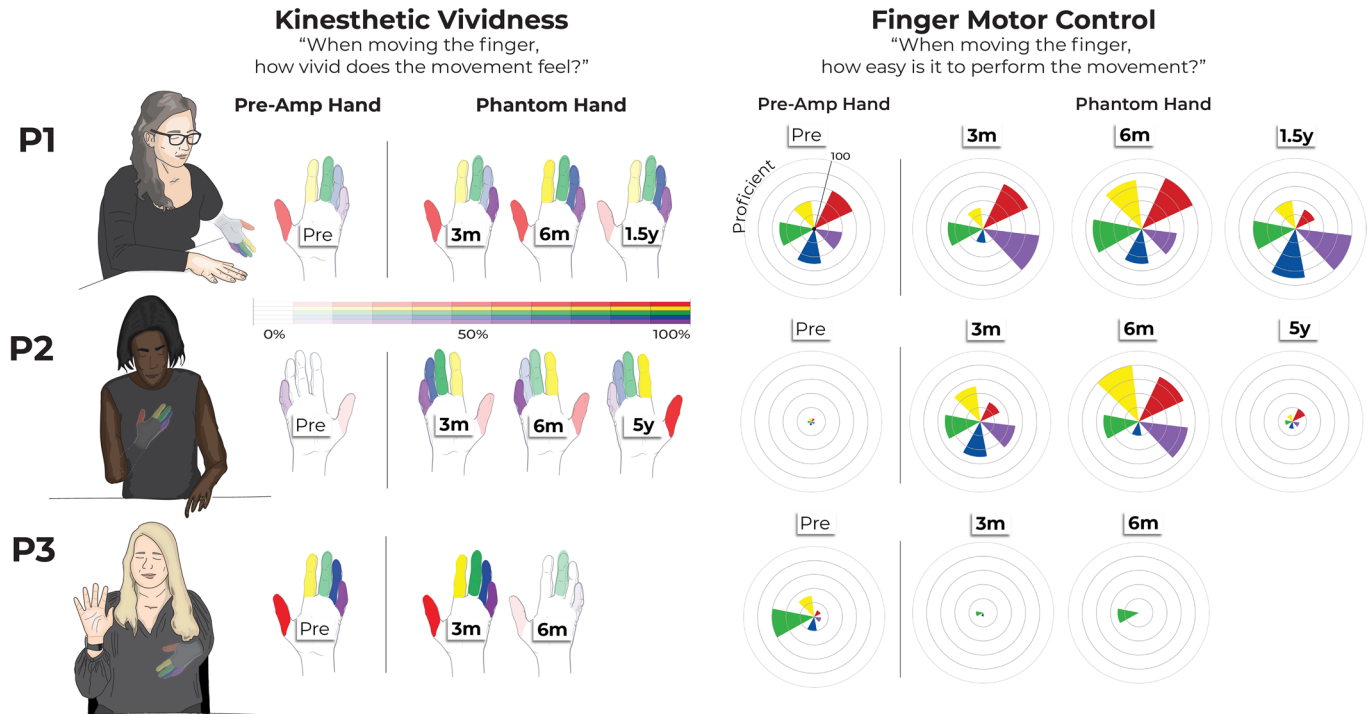
Supplementary information The online version contains supplementary material available at <https://doi.org/10.1038/s41593-025-02037-7>.

Correspondence and requests for materials should be addressed to Hunter R. Schone or Tamar R. Makin.

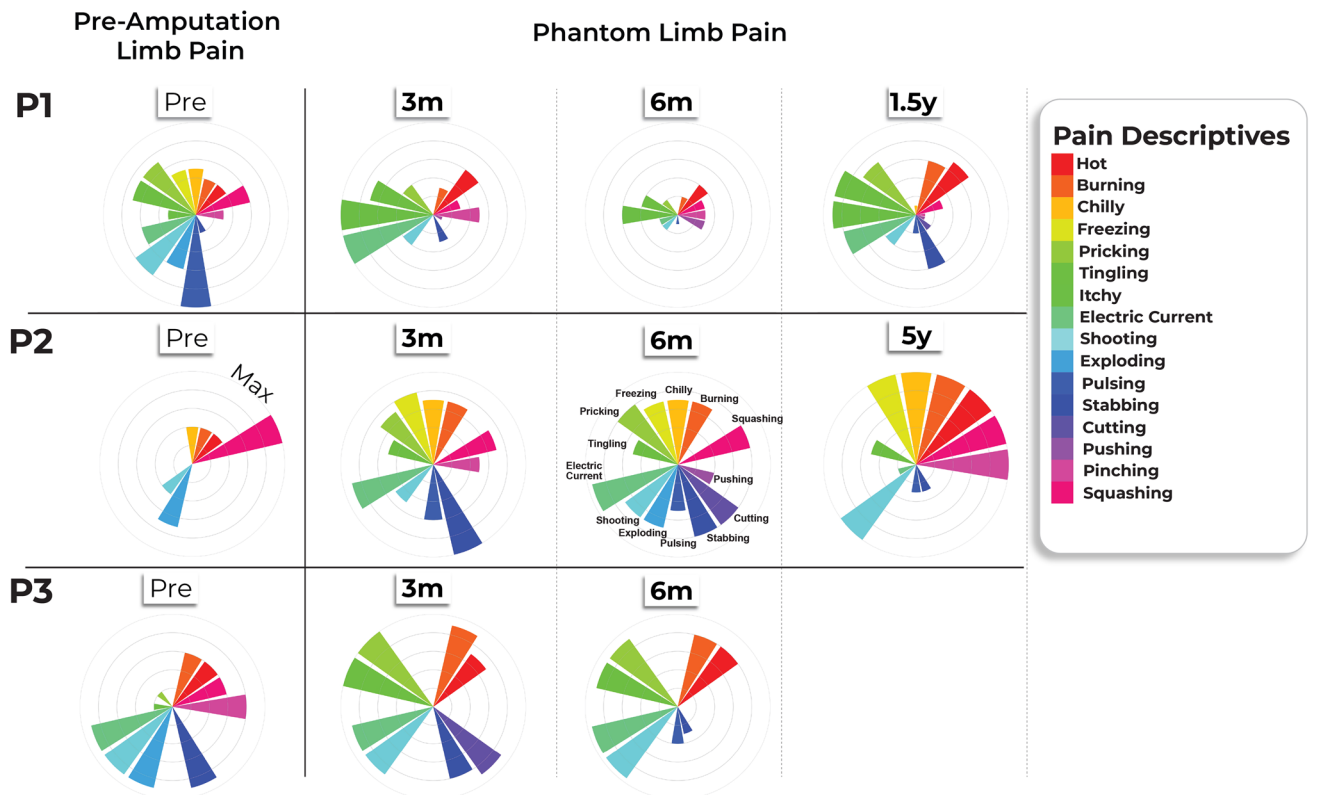
Peer review information *Nature Neuroscience* thanks the anonymous reviewer(s) for their contribution to the peer review of this work.

Reprints and permissions information is available at www.nature.com/reprints.

A Subjective feeling of fingers before and after amputation



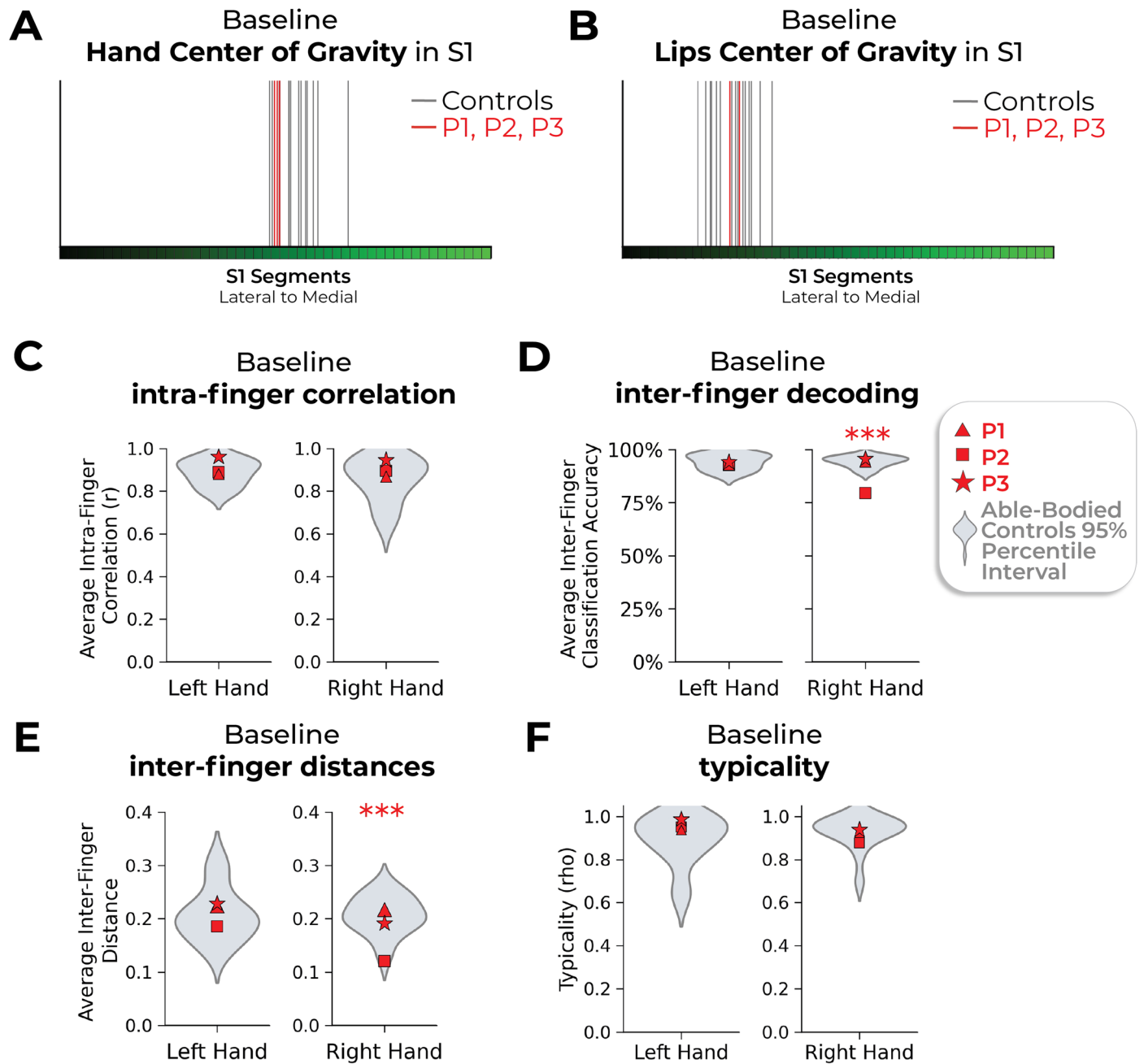
B Descriptives of limb pain before and after amputation



Extended Data Fig. 1 | See next page for caption.

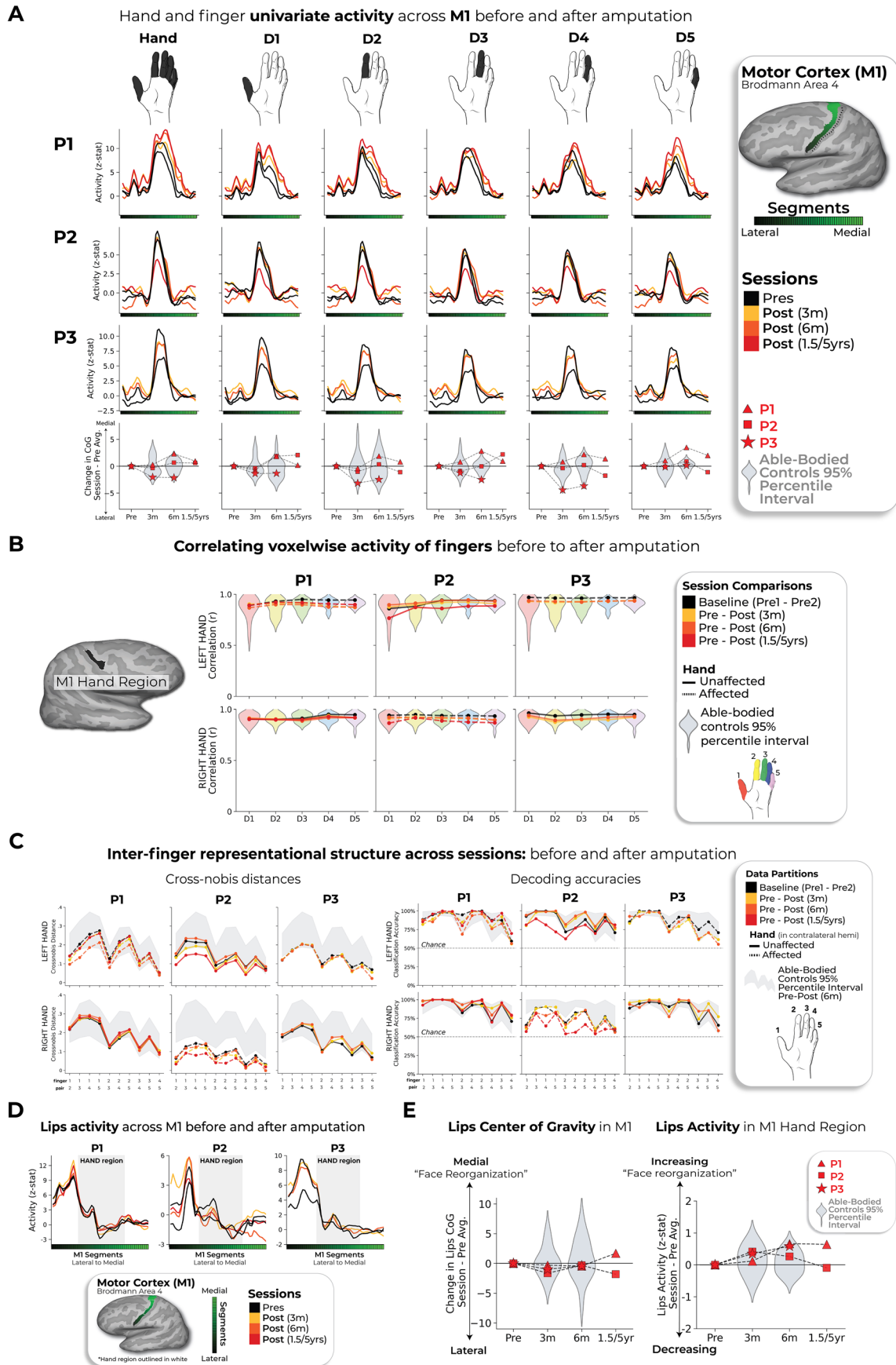
Extended Data Fig. 1 | Longitudinal characterization of finger sensations and limb pain. (a) Affected hand sensations before and after amputation. Finger vividness and motor control for the phantom fingers, relative to the pre-amputated fingers. Kinesthetic vividness rated on a scale from 0 (no sensation) to 100 (as vivid as the unaffected hand) with color intensity indicating level. Movement difficulty rated from 100 (as easy as the unimpaired hand) to 0 (extremely difficult). Finger colors: red=D1, yellow=D2, green=D3, blue=D4,

purple=D5 (palm excluded). (b) Before and after amputation, participants reported intensity values for each pain descriptive word, broadly categorized into sensations that are mechanical, temperature-related and other. For each word, participants were asked to describe the intensity between 0 (non-existing) to 100 (excruciating pain) as it relates to that particular word. A value of 100 (Max) is the largest radii on the polar plot. 3 M=3 months post-amputation; 6 M=6 months post-amputation. 1.5/5 yrs=1.5 or 5 years post-amputation.



Extended Data Fig. 2 | Baseline measures for the case-study participants that underwent an amputation versus able-bodied controls. Across all panels, we only report statistics when significant. Case-study participants showed similar responses to able-bodied controls in the baseline (pre-amputation) S1 center of gravity for the (a) hand and (b) lips. (c) All case-study participants had similar average intra-finger correlations between the two pre-sessions as controls.

For baseline average inter-finger (d) classification accuracy and (e) distances. One case-study participant exhibited lower values for their affected hand only, relative to controls [Crawford t-test: decoding and distances: P2: $p < 0.001$] (f) All case-study participants had similar hand typicality between the two pre-sessions as controls. All other annotations the same as described in Figs. 2 and 3.

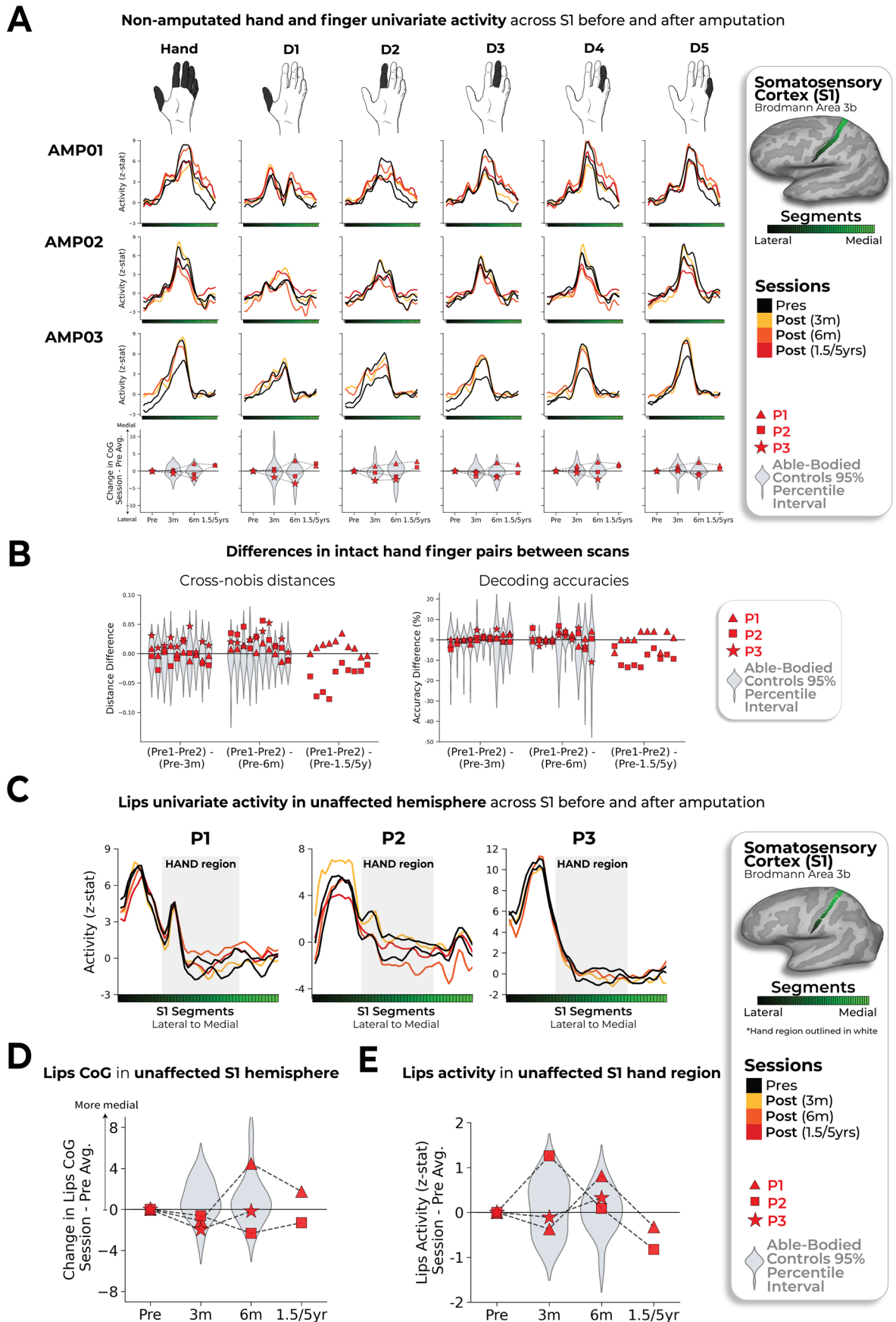


Extended Data Fig. 3 | See next page for caption.

Extended Data Fig. 3 | Replication of all primary results within motor cortex.

(a) Hand and finger univariate activity across M1 before and after amputation. When testing the stability of the whole hand condition across sessions, all case-studies fell within the distribution of controls at all timepoints. **(b)** When correlating voxel wise finger activity across sessions, all case-studies exhibiting similar correlation coefficients as controls, for all fingers. Please refer to the Extended Data Fig. 5 caption for a more detailed understanding of the correlation analysis. **(c)** Inter-finger representational structure across sessions, measured using cross-nobis distances (left) and decoding accuracies (right). First, when assessing for atypicality in our case-studies pre-amputation compared to controls, only case-study P2 exhibited reduced average finger selectivity pre-amputation based on the RSA (Crawford t-test: $t(15) = -3.15$, $p = 0.007$) and decoding ($t(15) = -3.9$, $p = 0.001$; similar to what was observed in S1). Next, when

testing for reductions in average finger selectivity at the 6-month timepoint, relative to baseline, only case-study P1 exhibited a significant reduction compared to controls [cross-nobis distances: 3 comparisons; $t(15) = 2.33$; $p_{\text{uncorr}} = 0.02$]; decoding: 3 comparisons; $t(15) = 2.32$; $p_{\text{uncorr}} = 0.03$]. However, it returned to the typical range when later assessed at the 1.5 year timepoint (for both measures). We also noted that case-study P3 showed a significant reduction at the 6-month timepoint, relative to controls, in the decoding (3 comparisons; $t(15) = 2.18$, $p_{\text{uncorr}} = 0.046$), but not the cross-nobis. **(d)** Lips univariate activity plotted across M1 before and after amputation. **(e)** All case studies showed typical session to session variability as controls in (left side) the lips center of gravity across M1 and (right side) lips activity in the M1 hand region. All annotations are the same as described in the captions of the Figs. 2–3 and Extended Data Fig. 5. Across all panels, we only report statistics when significant.



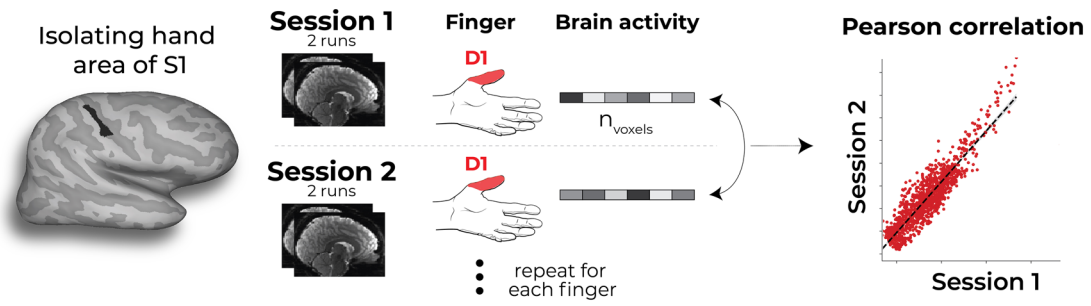
Extended Data Fig. 4 | See next page for caption.

Extended Data Fig. 4 | Stability of the intact (non-amputated) hand and lip topography in the non-affected hemisphere across amputation. (a) Intact hand and finger univariate activity across S1 before and after amputation. When testing the stability of the whole hand condition across sessions, all case-studies fell within the distribution of controls at all timepoints. (b) Unaffected (intact) hand between-session differences in inter-finger values. Difference values are depicted for the (left) cross-validated distances and (right) decoding accuracies. Classification/distance differences before and after amputation are visualized for each finger pair [Pre1-Pre2] minus [Pre Avg. - Post1 (3 m)] minus, [Pre1-Pre2] minus [Pre Avg. - Post2 (6 m)] and [Pre1-Pre2] minus [Pre Avg. - Post3 (1.55/y)]. Each violin plot reflects an individual finger pair (same order of finger-pairs as detailed in Fig. 2d). For consistency, the control values are all for the left-hand. When computing the session-to-session differences relative to controls, all

case-study participants showed typical session-to-session variability in finger selectivity at the 6-month timepoint, relative to controls. (c) Longitudinal lips univariate in the unaffected hemisphere (contralateral to intact hand) across S1 before and after amputation. (d) All case study participants showed typical changes in the lips center of gravity (CoG) in the unaffected S1 hemisphere across scans, relative to controls. (e) When testing for changes in lip activity (in the unaffected hand region), one case-study, P1, exhibited a significant atypical increase in lip activity relative to controls at the 6-month timepoint (Crawford t-test: $t(15) = 2.75$, $p_{\text{uncorr}} = 0.01$). However, the activity returned into the distribution of controls when tested at the 1.5 year timepoint ($t(15) = 0$, $p_{\text{uncorr}} = 0.99$). All other annotations are the same as described in Figs. 2 and 3. We only report statistics when significant.

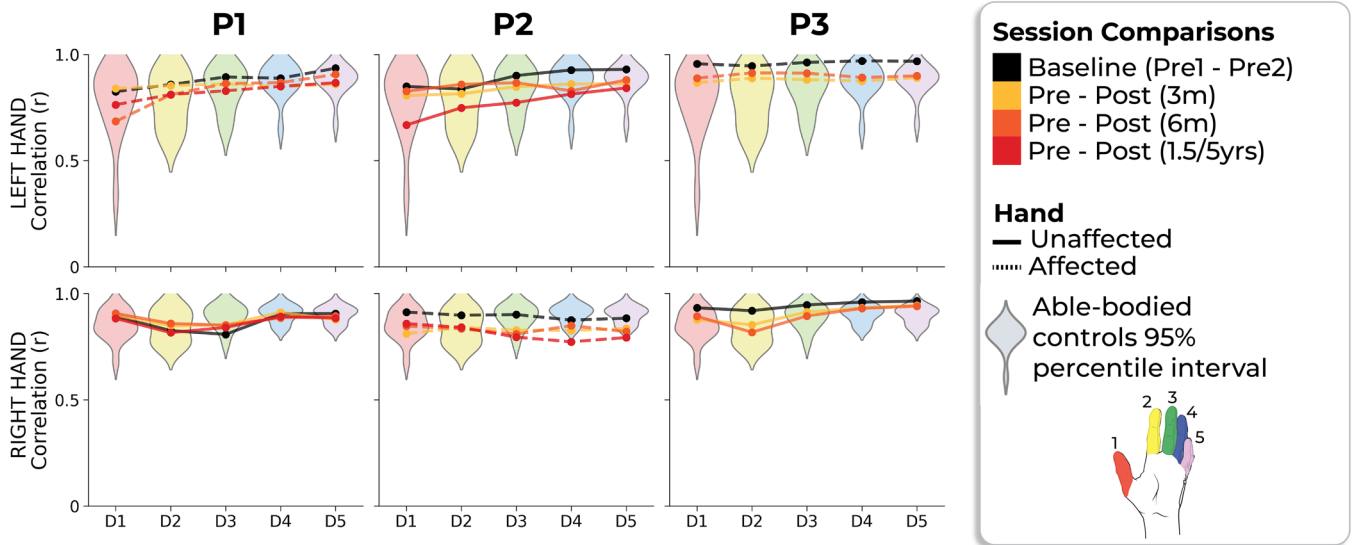
A

Correlating voxelwise activity of fingers before to after amputation



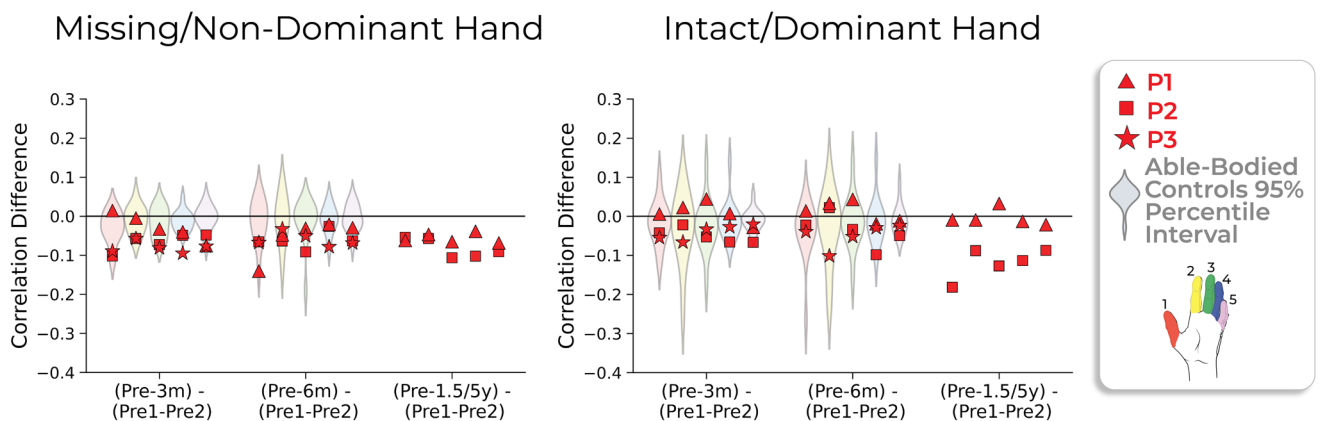
B

Finger correlation coefficients



C

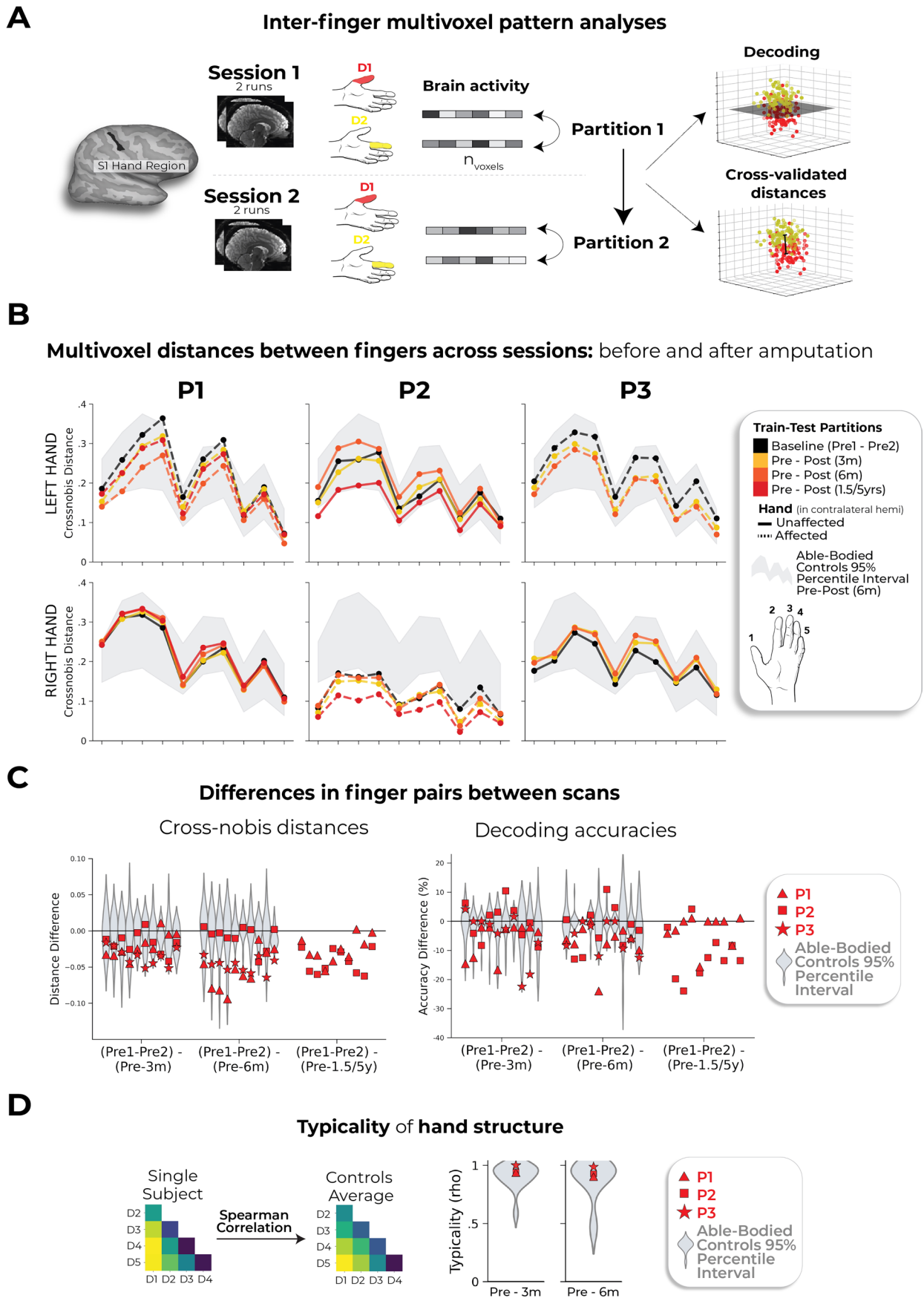
Changes in correlation coefficients across sessions



Extended Data Fig. 5 | See next page for caption.

Extended Data Fig. 5 | Correlating pre- to post-amputation multivoxel finger activity patterns. (a) Visualization depicting the inter-session Pearson correlations of individual fingers within the BA3b hand region. (b) Inter-session correlations for the left (top row) and right hands (bottom) in the contralateral hand ROI. Line colors indicate session pairings (indicated in the legend). For case-study participants, dashed line denotes the affected hand; solid line unaffected hand. Violin plots reflect able-bodied control's Pre – Post (6 m) values. (c) Between-session differences in finger correlation coefficients. Difference values are depicted for the (left) missing or non-dominant hand of controls and (right) intact or dominant hand of controls. The difference values are ordered to reflect the increasing gap between sessions: [Pre1-Pre2] minus [Pre Avg. – Post1

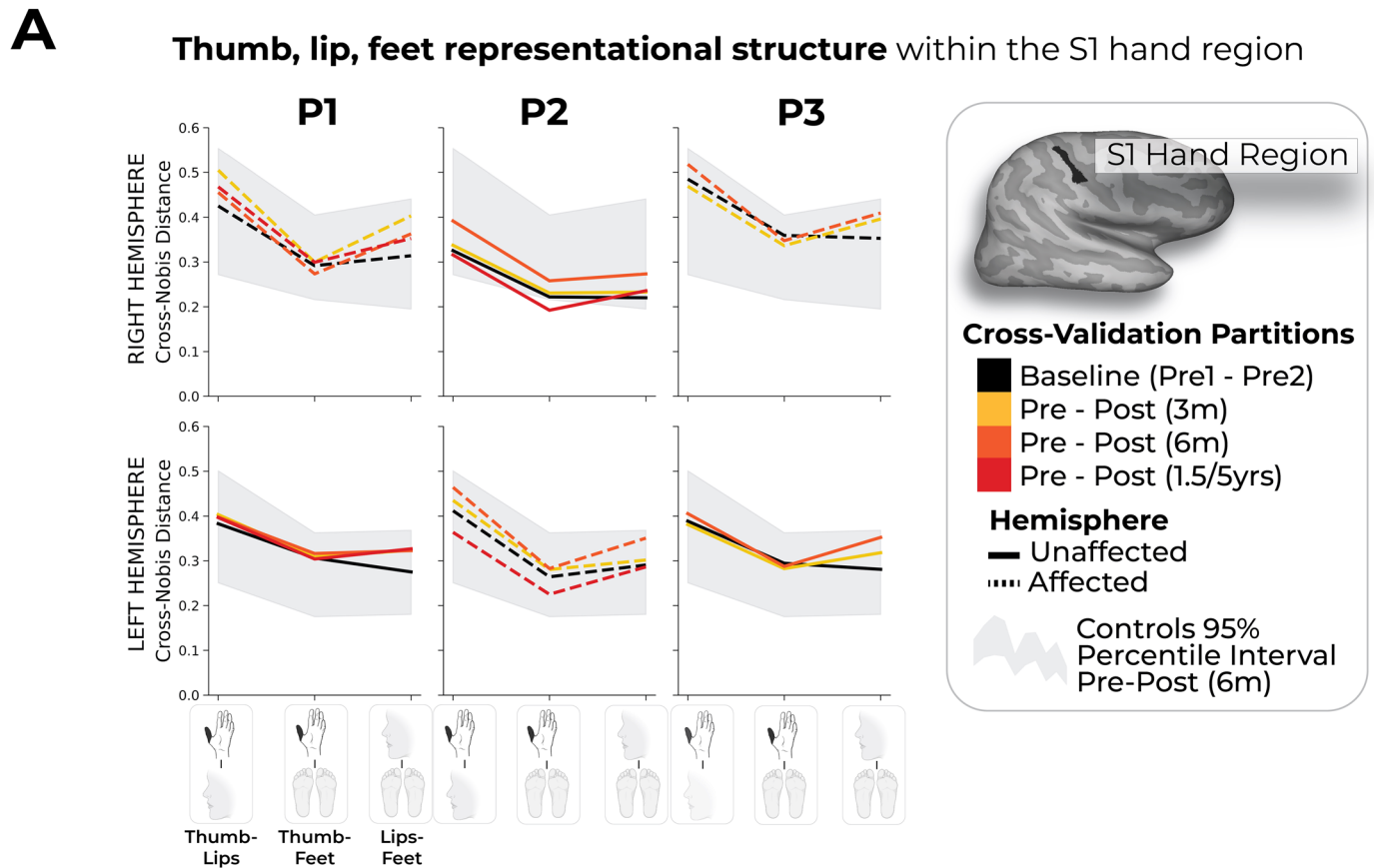
(3 m)] minus, [Pre1-Pre2] minus [Pre Avg. – Post2 (6 m)] and [Pre1-Pre2] minus [Pre Avg. – Post3 (1.55/y)]. Each violin plot reflects an individual finger. When testing whether the case-study participants showed a unique reduction in the average correlation, across fingers, relative to controls, for the missing hand, only P3, at the 3-month timepoint, for the missing hand (not intact), showed a significant pre-post reduction in the average correlation coefficient, relative to controls ($t(15) = -2.59$, $p_{\text{uncorr}} = 0.02$). However, this difference returned to the typical range of controls when later tested at the 6-month timepoint ($t(15) = -1.23$, $p_{\text{uncorr}} = 0.23$). All other annotations are as in Fig. 2. We only report statistics when significant.



Extended Data Fig. 6 | See next page for caption.

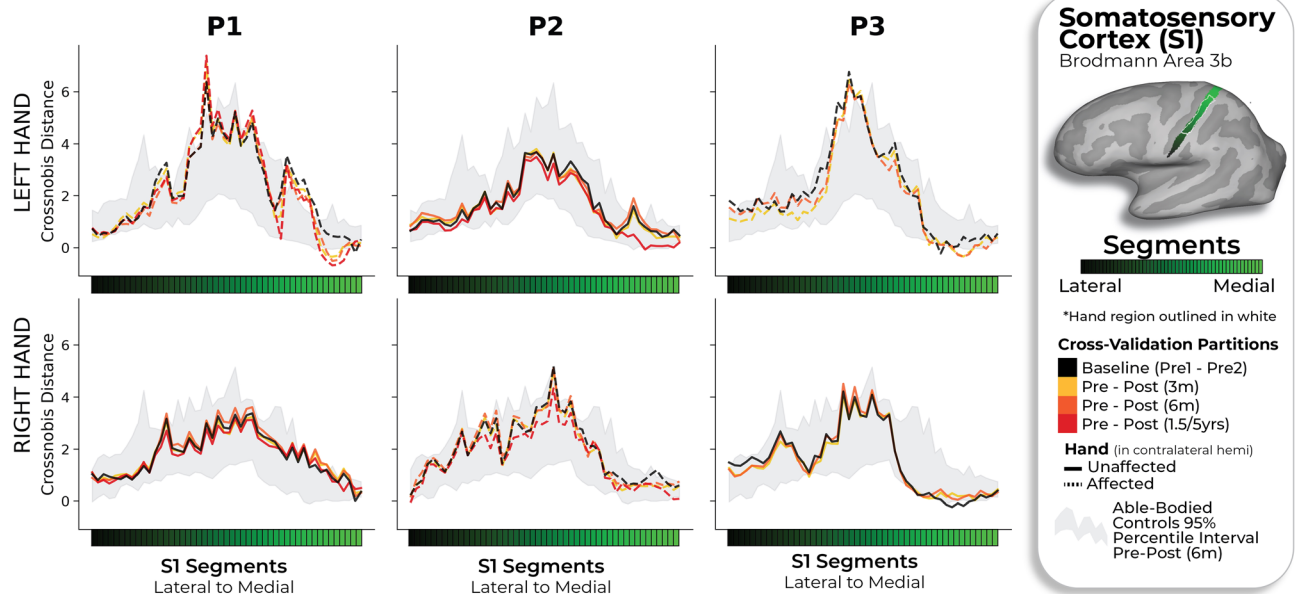
Extended Data Fig. 6 | Representational similarity analysis of inter-finger representational structure. (a) Graphic illustration of multivoxel pattern analyses. (b) Inter-finger multivariate analysis using cross-validated Mahalanobis (cross-nobis) distances. Line colors denote train-test/cross validation session pairs, respectively as indicated in the legend. The gray shaded area reflects able-bodied control's Pre – Post (6 m) data (95% percentile interval). (c) Classification/distance differences before and after amputation are visualized for each finger pair [Pre1-Pre2] minus [Pre Avg. – Post1 (3 m)] minus, [Pre1-Pre2] minus [Pre Avg. – Post2 (6 m)] and [Pre1-Pre2] minus [Pre Avg. – Post3 (1.55/y)]. Each violin plot reflects an individual finger pair (same order of finger-pairs as detailed in b). When comparing differences relative to controls, we observed some temporary, idiosyncratic reductions in average finger selectivity, relative to controls. First for the cross-nobis results, P1 showed a temporary reduction in average finger

selectivity at 6 months (3 comparisons; $t(15) = -2.79$, $p_{\text{uncorr}}=0.01$), though later offset to the typical range at their follow-up 1.5-year scan. P2 only exhibited reduced selectivity only at the 5-year timepoint, though reduction seen in the intact hand as well (Extended Data Fig. 4). Finally, P3 exhibited reduced selectivity at 6 months relative to controls (2 comparisons; $t(15) = -2.36$, $p_{\text{uncorr}}=0.03$). For the decoding results, P2 seemed to show significantly reduced selectivity at the 5-year timepoint, though also reduced for the intact hand (Extended Data Fig. 4). (d) The representational typicality of the hand structure was estimated by correlating each session's cross-validated Mahalanobis distances for each participant to a canonical inter-finger structure (controls average). All case-study participant's typicality values fell within the distribution of controls. All other annotations are as in Fig. 2. We only report statistics when significant.



B

Hand-lips multivoxel distance at every S1 segment cross-validated across sessions



Extended Data Fig. 7 | Thumb, lip and feet distances within the S1 hand region.

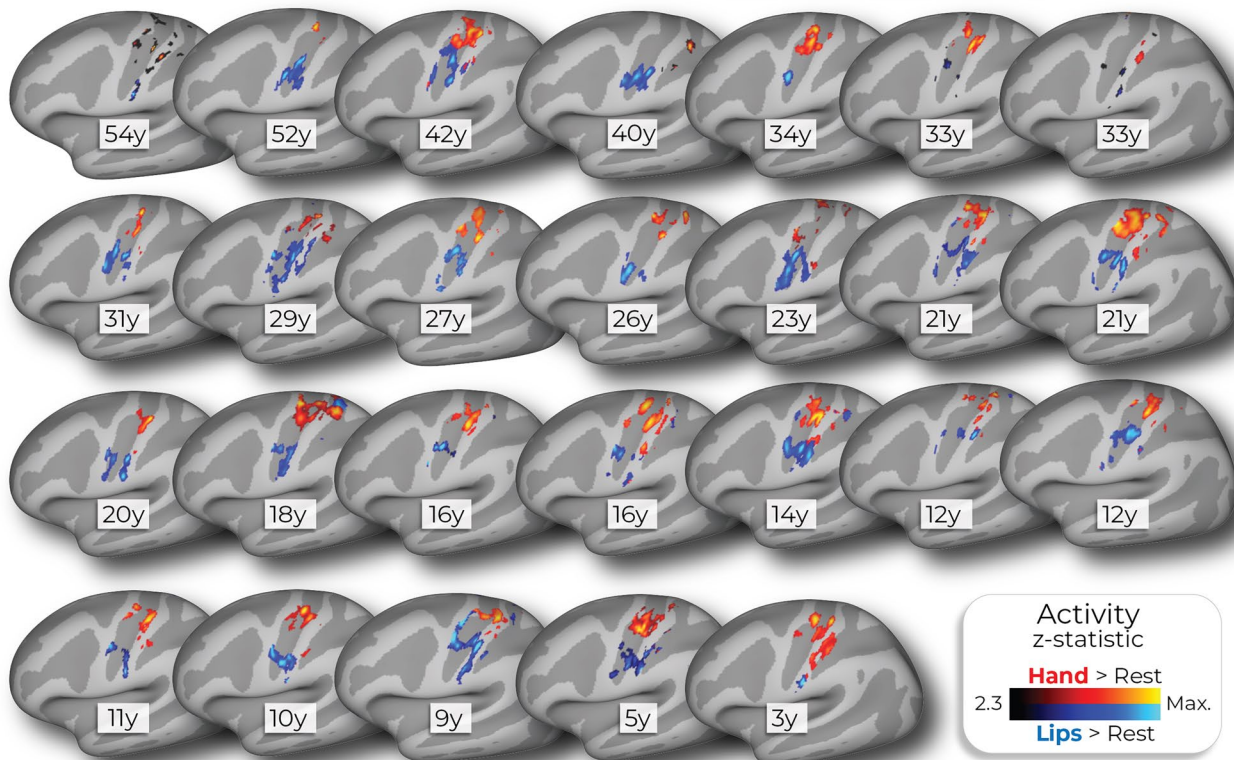
(a) Multivariate distances between the thumb, lip and feet cross-validated across sessions depicted for the right (top row) and left hemisphere (bottom) of the case-study participants that underwent an amputation and controls, contralateral to the thumb side being moved. Distances appear in the following order: (1) thumb-lips, (2) thumb-feet, (3) lips-feet. Line colors indicate session pairings (indicated in the legend). For case-study participants, dashed line denotes the

affected hemisphere; solid line unaffected hemisphere. Grey shaded area reflect able-bodied control's Pre - Post (6 m) values. For the affected hemisphere of the case-study participants, all distances fell within the typical range of the able-bodied controls. (b) We also tested whether changes occurred in the multivariate hand-lip distance when performed within each of the 49 S1 segments/ All case-study participants showed similar distances across sessions, before and after amputation. All other annotations are the same as described in Fig. 2.

Cross-sectional datasets

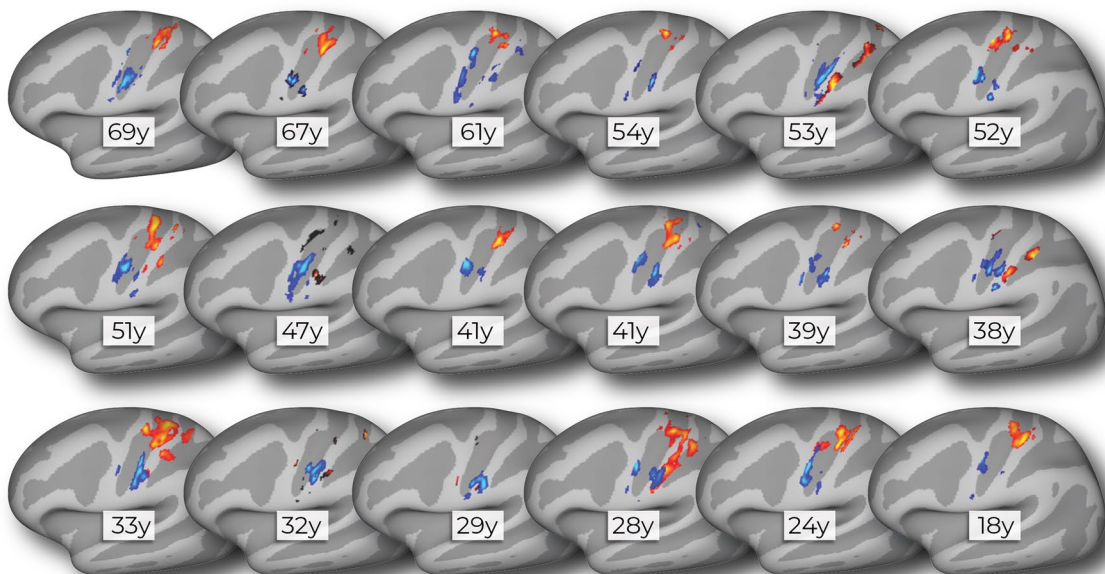
Phantom hand and lip cortical maps of chronic amputees (n=26)

Affected hand hemisphere | Ranked by "Years since amputation"



Non-dominant hand and lip cortical maps of able-bodied controls (n=18)

Hemisphere contralateral to non-dominant hand | Ranked by "Age"

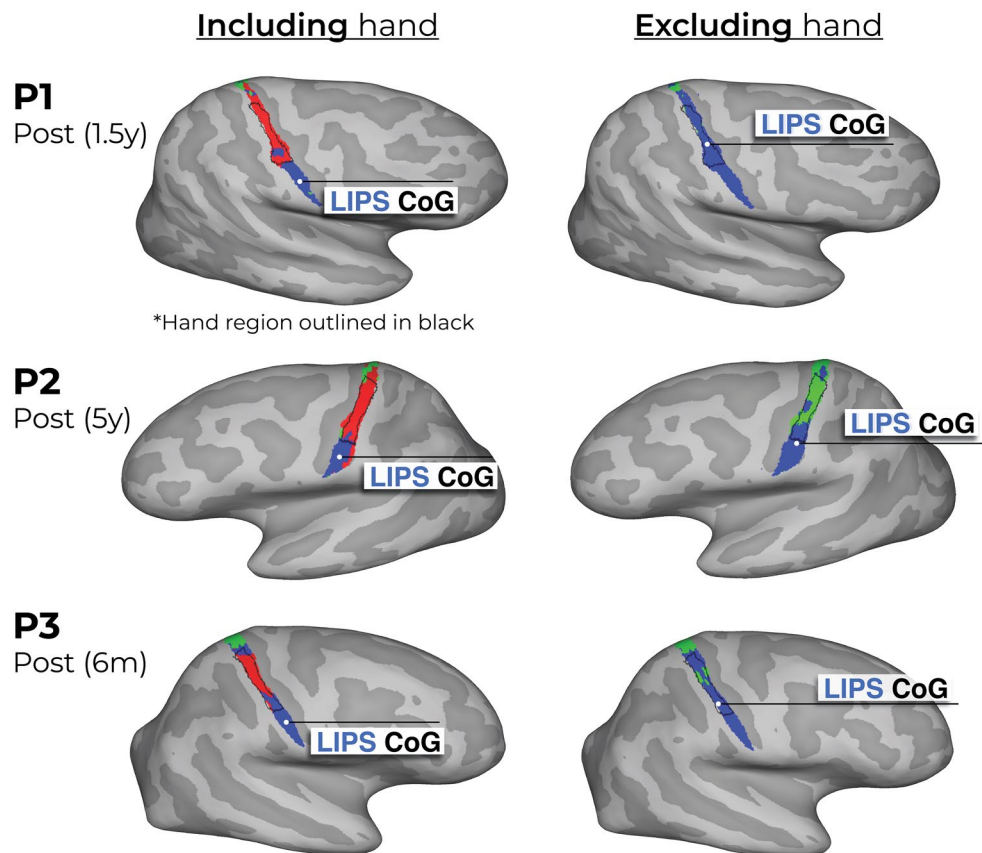


Extended Data Fig. 8 | See next page for caption.

Extended Data Fig. 8 | Hand and lip cortical maps of cross-sectional datasets.

Participant hand and lip cortical maps – registered to a standard cortical surface – are visualized for the chronic amputee participants (top row; $n = 26$) and secondary able-bodied control participants who underwent the same procedures as the chronic amputees ($n = 18$; bottom row). Hand maps for the amputees reflect moving their phantom hand, while for controls reflect moving

their non-dominant hand (in the contralateral hemisphere). All maps are contrasted against rest, minimally thresholded at 50% the maximum z-statistic and masked to Brodmann regions: 1, 2, 3a, 3b, and 4. Amputee maps are ranked by the numbers of years since amputation at the time of the scan and control maps are ranked by the participants age at the time of the scan.

Winner-takes-all analysis of the major body-parts across S1

Extended Data Fig. 9 | Winner-takes-all analysis of the major body parts (hand, lips and feet) across S1. Using the data from the last session of each participant, each voxel was awarded to the body-part with the highest response. Left column – we show the winner-takes-all analysis when performed on 3 body-parts: hand (red), lips (blue) and feet (green) versus (Right column) when excluding the physically absent hand. This comparison reveals supposed large-scale expansions of the lips or feet into the deprived hand region (black outline) post-amputation. We've also depicted the center of gravity (CoG) of the winner-takes-all lip cluster (white circles) to further demonstrate this. When excluding the

hand activity, the CoG of the lips 'shifts' towards the hand area. Thus, ignoring the primary body part – depending on your analysis choices – can substantially bias the results^{61,62}. Combined with the use of cross-sectional designs, this analysis approach has led to the impression of cortical remapping and even large-scale reorganization of the lip representation following amputation. Crucially, the newly assigned winner in the hand area [left panel] has rarely been directly compared against the persistent representation of the missing hand, and indeed, indicative evidence show that this recorded activity in the hand area is weak (we extensively discuss this in our recent review ref. 17).

Extended Data Table 1 | Demographics of the case study participants who underwent an amputation

	P1	P2	P3
Sex	Female	Female	Female
Age (at first scan)	26	57	49
Handedness at birth	Left-handed	Right-handed	Right-handed
Cause of amputation	Arteriovenous vascular malformation (AVM)	Sarcoma tumour	Severell-Martorell syndrome led to multi-fractured arm with bones not healing
Disability duration	AVM progressed over a few years	Tumour slowly developing since 1995	Musculoskeletal issues since childhood
Amputated limb	Left upper limb	Right upper limb	Left upper limb
Level of amputation	Transhumeral	At elbow	Transhumeral
Amputation surgery	Combination of targeted muscle reinnervation and regenerative peripheral nerve interfaces, see Supplementary Figure 2 .	Traditional: sharply transected the nerves and allowed to retract	Traditional: sharply transected the nerves and allowed to retract
Phantom position and mobility	Phantom hand positioned slightly above the elbow; only feels the hand, not the forearm; can move all phantom fingers (Figure 1B).	Phantom hand positioned upright towards chest; only feels the hand, not the forearm; can move all phantom fingers (Figure 1B).	Phantom hand positioned upright towards chest; mostly hand and fingers (little elbow); can move all phantom fingers (Figure 1B).
When did phantom sensations occur	Immediately after amputation	Immediately after amputation	Immediately after amputation
Phantom limb sensation (PLS) intensity (100 max) (3m, 6m, 1.5/5yrs respectively)	40, 60, 40	90, 100, 100	100, 90, NA
PLS frequency (3m, 6m, 1.5/5yrs)	3m: once a week; 6m: several times per month; 1.5yr: once or less per month	3m: all the time; 6m: all the time; 5yrs: all the time	3m: all the time; 6m: daily
Chronic PLS (100 max) (3m, 6m, 1.5/5yrs)	13.3, 15, 8	90, 100, 100	100, 45, NA
Limb pain intensity (Pre, 3m, 6m, 1.5/5yrs)	90, 20, 0, 0	80, 50, 70, 70	50, 80, 70, NA
Limb pain frequency (Pre, 3m, 6m, 1.5/5yrs)	Pre: all the time; 3m: several times per month; 6m: once or less per month; 1.5yr: once or less per month	Pre: all the time; 3m: daily; 6m: daily; 5yrs: all the time	Pre: daily; 3m: daily; 6m: once a week
Chronic limb pain (Pre, 3m, 6m, 1.5/5yrs)	90, 5, 0, 0	80, 25, 35, 70	25, 40, 23.3, NA
Transient (on the day) limb pain (Pre, 3m, 6m, 1.5/5yrs; 100 max) (Pre, 3m, 6m, 1.5/5yrs)	50, 30, 0, 0	80, 45, 50, 70	50, 40, 20, NA
Pain Detect Score (% max possible score) (Pre, 3m, 6m, 1.5/5yrs)	51%, 34%, 14%, 40%	68%, NA, 42%, 45%	65%, 65%, 65%, NA
Pain Detect Pain Course	- Persistent pain with pain attacks (Same pre and 3m) - Persistent pain with slight fluctuations (6m, 1.5yrs)	- Persistent pain with pain attacks (Same pre and 6m) - Persistent pain with slight fluctuations (5yrs)	- Pain attacks with pain between them (pre) - Persistent pain with pain attacks (3m) - Pain attacks without pain between them (6m)
Upper Extremity Functional Index (Pre, 3m, 6m, 1.5/5yrs) 100% = no impairment	47%, 23%, 36%, 57%	30%, NA, 11%, 28%	0%, 39%, 69%, NA
Prosthesis Type	None	None (fitted with a cosmetic prosthesis)	Cosmetic prosthesis
Prosthesis Use	None	None. Briefly used in the first 6 months post-amputation (2 days a week, ~2 hours a day)	6m: 2 days a week, 8 hours a day

PLS = phantom limb sensation; Limb pain reflects pre-amputation limb pain or post-amputation phantom limb pain. Frequency scores: 1 – all the time, 2 – daily, 3 – weekly, 4 – several times per month, and 5 – once or less per month. Chronic pain/sensation values were calculated by dividing intensity by frequency. NA = not available/applicable. Upper extremity functional index measures participant difficulty with performing activities due to their missing limb.

Reporting Summary

Nature Portfolio wishes to improve the reproducibility of the work that we publish. This form provides structure for consistency and transparency in reporting. For further information on Nature Portfolio policies, see our [Editorial Policies](#) and the [Editorial Policy Checklist](#).

Statistics

For all statistical analyses, confirm that the following items are present in the figure legend, table legend, main text, or Methods section.

- | n/a | Confirmed |
|--------------------------|--|
| <input type="checkbox"/> | <input checked="" type="checkbox"/> The exact sample size (n) for each experimental group/condition, given as a discrete number and unit of measurement |
| <input type="checkbox"/> | <input checked="" type="checkbox"/> A statement on whether measurements were taken from distinct samples or whether the same sample was measured repeatedly |
| <input type="checkbox"/> | <input checked="" type="checkbox"/> The statistical test(s) used AND whether they are one- or two-sided
<i>Only common tests should be described solely by name; describe more complex techniques in the Methods section.</i> |
| <input type="checkbox"/> | <input checked="" type="checkbox"/> A description of all covariates tested |
| <input type="checkbox"/> | <input checked="" type="checkbox"/> A description of any assumptions or corrections, such as tests of normality and adjustment for multiple comparisons |
| <input type="checkbox"/> | <input checked="" type="checkbox"/> A full description of the statistical parameters including central tendency (e.g. means) or other basic estimates (e.g. regression coefficient) AND variation (e.g. standard deviation) or associated estimates of uncertainty (e.g. confidence intervals) |
| <input type="checkbox"/> | <input checked="" type="checkbox"/> For null hypothesis testing, the test statistic (e.g. F , t , r) with confidence intervals, effect sizes, degrees of freedom and P value noted
<i>Give P values as exact values whenever suitable.</i> |
| <input type="checkbox"/> | <input checked="" type="checkbox"/> For Bayesian analysis, information on the choice of priors and Markov chain Monte Carlo settings |
| <input type="checkbox"/> | <input checked="" type="checkbox"/> For hierarchical and complex designs, identification of the appropriate level for tests and full reporting of outcomes |
| <input type="checkbox"/> | <input checked="" type="checkbox"/> Estimates of effect sizes (e.g. Cohen's d , Pearson's r), indicating how they were calculated |

Our web collection on [statistics for biologists](#) contains articles on many of the points above.

Software and code

Policy information about [availability of computer code](#)

Data collection

Data analysis

For manuscripts utilizing custom algorithms or software that are central to the research but not yet described in published literature, software must be made available to editors and reviewers. We strongly encourage code deposition in a community repository (e.g. GitHub). See the Nature Portfolio [guidelines for submitting code & software](#) for further information.

Data

Policy information about [availability of data](#)

All manuscripts must include a [data availability statement](#). This statement should provide the following information, where applicable:

- Accession codes, unique identifiers, or web links for publicly available datasets
- A description of any restrictions on data availability
- For clinical datasets or third party data, please ensure that the statement adheres to our [policy](#)

Research involving human participants, their data, or biological material

Policy information about studies with [human participants or human data](#). See also policy information about [sex, gender \(identity/presentation\), and sexual orientation](#) and [race, ethnicity and racism](#).

Reporting on sex and gender	The participants who underwent planned hand amputations included 3 volunteers: P1 [female; age = 26; lefthanded; left transhumeral amputation], P2 [female; age = 57; left-handed; right at elbow amputation], P3 [female; age = 49; right-handed; left transhumeral amputation], were recruited through the National Health Service. The longitudinal able-bodied control group included 16 able-bodied volunteers [9 females; mean age \pm std = 53.1 \pm 6.37; all right-handed]. The chronic amputee group included 26 upper-limb amputee volunteers [4 females; mean age \pm std = 51.1 \pm 10.6; 13 missing left upper-limb; level of amputation: 17 transradial, 8 transhumeral and 1 at wrist; mean years since amputation \pm std = 23.5 \pm 13.5], which were recruited through the NHS. The secondary able-bodied control group included 18 able-bodied volunteers [7 females; mean age \pm std = 43.1 \pm 14.62; 11 right-handed]. Information on sex was self-reported by the volunteers. All able-bodied participants were recruited through University College London and the London metro area.
Reporting on race, ethnicity, or other socially relevant groupings	Not applicable
Population characteristics	See above.
Recruitment	All amputee participants were recruited via NHS participant identification centres. There were no self-selection biases that would impact our results. All able-bodied participants were recruited through University College London and the London metro area.
Ethics oversight	The study and its experimental procedures were approved by the NHS National Research Ethics Committee (18/LO/0474).

Note that full information on the approval of the study protocol must also be provided in the manuscript.

Field-specific reporting

Please select the one below that is the best fit for your research. If you are not sure, read the appropriate sections before making your selection.

Life sciences Behavioural & social sciences Ecological, evolutionary & environmental sciences

For a reference copy of the document with all sections, see [nature.com/documents/nr-reporting-summary-flat.pdf](https://www.nature.com/documents/nr-reporting-summary-flat.pdf)

Behavioural & social sciences study design

All studies must disclose on these points even when the disclosure is negative.

Study description	Quantitative experimental
Research sample	"The participants who underwent planned hand amputations included 3 volunteers: P1 [female; age = 26; left-handed; left transhumeral amputation], P2 [female; age = 57; left-handed; right at elbow amputation], P3 [female; age = 49; right-handed; left transhumeral amputation], were recruited through the National Health Service. The longitudinal able-bodied control group included 16 able-bodied volunteers [9 females; mean age \pm std = 53.1 \pm 6.37; all right-handed]. The chronic amputee group included 26 upper-limb amputee volunteers [4 females; mean age \pm std = 51.1 \pm 10.6; 13 missing left upper-limb; level of amputation: 17 transradial, 8 transhumeral and 1 at wrist; mean years since amputation \pm std = 23.5 \pm 13.5], which were recruited through the NHS. The secondary able-bodied control group included 18 able-bodied volunteers [7 females; mean age \pm std = 43.1 \pm 14.62; 11 right-handed]. Due to the rarity of identifying and testing participants pre-amputation, the sample size was based on the total number of amputees that could be successfully recruited. The researcher was not blinded to experimental condition and/or the study hypothesis."
Sampling strategy	Due to the rarity of identifying and testing participants pre-amputation, the sample size was based on the total number of amputees that could be successfully recruited.
Data collection	"There 3 data-types reported in the study: (1) fMRI data, (2) kinematic data and (3) questionnaire data. MRI images were obtained using a 3-Tesla Prisma scanner (Siemens, Erlangen, Germany) with a 32-channel head coil. Kinematic data was acquired by video recordings using 4 Logitech brio cameras. Questionnaire data was acquired via paper and pen. For all sessions, a single researcher and the research participant were present."
Timing	All data collection took place between May 4, 2019 to May 17, 2024.
Data exclusions	No data were excluded.
Non-participation	Over a 7-year period and across multiple NHS sites in the UK, we recruited 18 potential patients preparing to undergo hand amputations. Due to a multitude of factors (e.g., MRI safety contraindications, no hand motor control, age outside ethics, high level

of disability), we could only perform pre-amputation testing on 6 patients. Due to additional factors (complications during surgery, general health, retractions) we successfully completed our full testing procedure on 3 patients. For the able-bodied controls, 4 volunteers did not complete their testing, due to drop-out and incidental findings captured in the MRI sessions.

Randomization

No randomization was performed because all participants underwent the same testing procedures.

Reporting for specific materials, systems and methods

We require information from authors about some types of materials, experimental systems and methods used in many studies. Here, indicate whether each material, system or method listed is relevant to your study. If you are not sure if a list item applies to your research, read the appropriate section before selecting a response.

Materials & experimental systems

n/a	Involvement in the study
<input checked="" type="checkbox"/>	<input type="checkbox"/> Antibodies
<input checked="" type="checkbox"/>	<input type="checkbox"/> Eukaryotic cell lines
<input checked="" type="checkbox"/>	<input type="checkbox"/> Palaeontology and archaeology
<input checked="" type="checkbox"/>	<input type="checkbox"/> Animals and other organisms
<input checked="" type="checkbox"/>	<input type="checkbox"/> Clinical data
<input checked="" type="checkbox"/>	<input type="checkbox"/> Dual use research of concern
<input checked="" type="checkbox"/>	<input type="checkbox"/> Plants

Methods

n/a	Involvement in the study
<input checked="" type="checkbox"/>	<input type="checkbox"/> ChIP-seq
<input checked="" type="checkbox"/>	<input type="checkbox"/> Flow cytometry
<input checked="" type="checkbox"/>	<input type="checkbox"/> MRI-based neuroimaging

Plants

Seed stocks

Report on the source of all seed stocks or other plant material used. If applicable, state the seed stock centre and catalogue number. If plant specimens were collected from the field, describe the collection location, date and sampling procedures.

Novel plant genotypes

Describe the methods by which all novel plant genotypes were produced. This includes those generated by transgenic approaches, gene editing, chemical/radiation-based mutagenesis and hybridization. For transgenic lines, describe the transformation method, the number of independent lines analyzed and the generation upon which experiments were performed. For gene-edited lines, describe the editor used, the endogenous sequence targeted for editing, the targeting guide RNA sequence (if applicable) and how the editor was applied.

Authentication

Describe any authentication procedures for each seed stock used or novel genotype generated. Describe any experiments used to assess the effect of a mutation and, where applicable, how potential secondary effects (e.g. second site T-DNA insertions, mosaicism, off-target gene editing) were examined.